Technical Document 1752
January 1990

Radio Refractivity Profiles Deduced From Lidar Measurements

M. R. Paulson
H. G. Hughes

NAVAL OCEAN SYSTEMS CENTER

San Diego, California 92152-5000

J. D. FONTANA, CAPT, USN
Commander

R. M. HILLYER
Technical Director

ADMINISTRATIVE INFORMATION

The work reported here was performed by members of the Tropospheric Branch, Ocean and Atmospheric Sciences Division, with funding provided by the NOSC block program *Battle Group Environmental Enhancement*.

Released by
H. V. Hitney, Head
Tropospheric Branch

Under authority of
J. H. Richter, Head
Ocean and Atmospheric
Sciences Division

ACKNOWLEDGMENT

The authors are grateful to R. A. Paulus, Tropospheric Branch, for providing the computer programs to record and process the radiosonde data.

CONTENTS

FIGURES

CONTENTS (continued)

TABLES

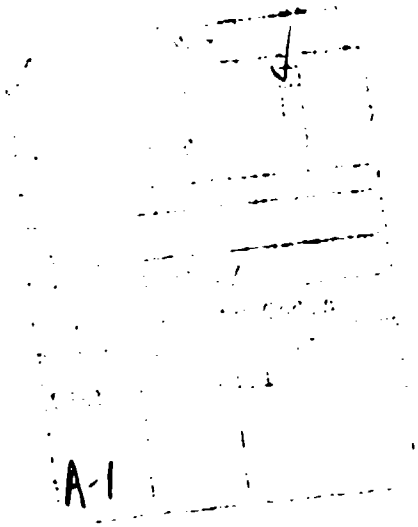

INTRODUCTION

A lidar (light detection and ranging) consists of a very short pulse of laser energy. The intensity of the laser energy scattered back to a receiver by atmospheric aerosols is recorded as a function of time, and therefore distance. The relative intensity of the light received from a given distance depends on the size, shape, and composition of the aerosols, both at that distance and along the intervening path.

Relative humidity can have a pronounced effect on the atmospheric aerosols. As the relative humidity increases, condensation of water vapor on particles containing water-soluble material causes the size and index of refraction of these particles to change (Fitzgerald, 1984). This causes the backscatter coefficient to increase with increasing relative humidity.

Since radio refractivity is also strongly dependent on relative humidity, it may be possible to use a lidar to get a measure of radio refractivity profiles. Of particular interest would be profiles indicating low-level and surface duct conditions.

A lidar has been used to measure the intensity of backscattered laser light as a function of altitude. The lidar (known as a visioceilometer) was a modified AN/GVS-5 laser rangefinder. This lidar operates at 1.06 μm with a nominal pulse energy of 13 mJ. The pulse half-width is 6 ns and the sampling rate is 20 MHz. This provides a sample every 7.5 meters. Table 1 lists additional characteristics of the lidar, as given by Lentz (1982). Some of these characteristics may have changed slightly since this table was produced.

Table 1. Characteristics of the visioceilometer lidar.

Beam divergence	1.0 mrad
Receiver field of view	3.0 mrad
Laser energy	13 mJ at 1.06 μm
Pulse half-width	6 ns
Receiver aperture	50 mm
Laser exit diameter	16 mm
Optics axis separation	50 mm
Full crossover range	80 m
Log A slope	10 mV/dB
Log A zero	80 μV
Detector noise level	2×10^{-10} W
Laser monitor output	0.75 ± 0.25 V
Sample rate	20 MHz
A/D converter	10 bits in 2 μs
Sample device	455-sample dual-channel CCD (Fairchild #CCD 321)
Operating temperature	-5° to 60°C (prototype)
Sample range	3.3 km

When the lidar is operated in the vertical direction in the presence of a cloud layer, a profile of the range-compensated backscattered signal, S(R), shows rapid increase in returned signal near the base of the cloud. This is a result of the increased backscatter from the cloud particles. A rapid decrease in returned signal follows as the signal penetrates the cloud and is attenuated. Figure 1 shows an example of this.

When an inversion exists, and if no clouds are present, the lidar return shows a very rapid decrease at the height of the inversion, as shown in figure 2. This results from a decrease in the backscattered signal

above the inversion, rather than from increased extinction. This decrease in backscattered signal corresponds to, and results from, a decrease in relative humidity through the inversion. An example of this is shown in figure 3.

Since tropospheric ducting of radiowaves is also a result of atmospheric inversions, it would be of interest to investigate whether lidar returns could be used to predict the presence, or absence, of ducting conditions. Of particular interest are low-level and surface-based ducts.

While the use of radiosondes is an established and standard method of determining the presence and location of ducts, there may be times when it is necessary to know whether ducting conditions exist but when radio signals transmitted from a radiosonde cannot be permitted. Furthermore, not all ships have radiosonde capability and this might help fill a need.

This type of remote sensor of refractivity profiles would also permit more frequent assessment of conditions.

MEASUREMENTS

The measurements were made at the southern tip of Point Loma in San Diego. This site is about 30 meters above sea level. The lidar was pointed in the vertical direction and 5 or 6 raw data profiles were recorded. A balloon-borne radiosonde was launched at the same time and temperature, pressure, and relative humidity were recorded as functions of time as the balloon rose. Measurements were made on an irregular basis. They were started on 12 September 1989 and ended on 21 November 1989. Usually, only one balloon launch was made on any given day. The dates when measurements were made are shown in table 2.

Table 2. Least-squares curve fit to a straight line for relative humidity as a function of lidar S(R) return. Curve is $Rh = A + B \cdot S(R)$.

Date	A	B	Correlation	Maximum Altitude
09/12/89	241.481	28.390	0.9477	1170
09/13/89	178.081	20.755	0.9243	728
09/18/89	218.973	21.564	0.7225	660
09/20/89	226.310	22.770	0.9305	608
09/26/89	270.510	34.270	0.9477	690
09/27/89	305.381	35.382	0.9613	1050
09/28/89	304.918	34.061	0.9315	420
09/29/89	186.333	17.823	0.8232	705
10/02/89	234.921	25.084	0.9417	1343
10/03/89	328.397	42.097	0.9733	1050
10/24/89	161.510	12.123	0.9452	600
11/13/89	219.892	22.416	0.7199	750
11/21/89	378.925	48.379	0.8534	1100

There was at least one important difference between the two types of measurements. While each lidar data profile was essentially a snapshot of conditions at the moment, the balloon-borne radiosonde rose about 200 meters per minute. In addition, there was frequently a fairly strong wind blowing that caused the balloon to drift rapidly, usually southeast over land, during its rise. This could result in the lidar and the radiosonde seeing somewhat different atmospheric conditions.

DATA ANALYSIS

LIDAR DATA PROCESSING

A curve, determined from calibration measurements, was used to adjust the raw lidar data. The curve consisted of a fifth-order fit to the calibration data. The resulting data were then adjusted to compensate for the range-square loss owing to distance. This provided a profile of range-compensated signal, S(R), as a function of altitude. A 9-point running average of the S(R) data for each profile was used in the comparison with the radiosonde data. This was done because the lidar frequently showed small-scale irregularities that the radiosonde did not detect because of a longer sensor response time.

Below about 100 meters altitude, the lidar curves show a rapid decrease. This occurs because the laser beam inside this distance is not completely in the field of view of the lidar receiver. In addition, above a certain altitude the lidar return approached the background noise level. This altitude depended on atmospheric conditions. It ranged from about 600 meters to 1100 meters on various days.

RADIOSONDE DATA PROCESSING

The radiosonde provided a record of temperature, pressure, and relative humiity as a function of time. These data were used to calculate altitude and refractivity. Profiles of relative humidity versus altitude, temperature versus altitude, and M-units versus altitude were generated from these data.

LIDAR S(R) VERSUS RELATIVE HUMIDITY PROFILES

The lidar provides an S(R) value every 7.5 meters of altitude. These S(R) values were plotted on the horizontal axis for each altitude, and relative humidity for the corresponding altitude was plotted on the vertical axis. Figure 4 is an example of these plots. Others are shown in the appendix.

A least-squares fit to a straight line was calculated for each profile. Table 2 is a list of these. Usually, the results show very good correlation between relative humidity and the lidar return for each case. However, the curve fit for 1 day can be quite different from that for another day. This probably occurs because the composition, or makeup, of the atmospheric aerosols can vary with time and with the direction of the wind.

All of the data have also been plotted on one graph to get an idea of the extent of this variability. This is shown in figure 5. Then a least-squares fit to a straight line was calculated for the data. The equation for this line was used to calculate relative humidity profiles from the various lidar returns.

LIDAR M-UNIT PROFILES VERSUS RADIOSONDE M-UNIT PROFILES

Relative humidity profiles were calculated from the lidar returns for each of the test days. These relative humidity profiles were used along with standard-lapse-rate profiles of temperature and pressure (referenced to surface measurements) to calculate an M-unit profile for each of the test days. The refractivity profiles were then compared to corresponding profiles calculated from the radiosonde data. Figure 6 shows two examples of these (others are found in the appendix). The continuous line is for the radiosonde and the dashed line is for the lidar.

COMPARISON OF SIGNAL COVERAGE PREDICTIONS

Ray-trace diagrams give qualitative, systems-independent appraisals of propagation conditions that are adequate to the needs of this report. More sophisticated propagation models would generally be required to assess effects on specific electromagnetic systems.

A Ray-trace computer program in a program called Engineer's Refractive Effects Prediction System (EREPS) by Hitney et al. (1988) was used to calculate and plot radio signal coverage for the radiosonde refractivity profile and for the lidar refractivity profile. Figure 7 shows these for 12 September 1989, with an inversion near 600 meters altitude. The upper graph is for the radiosonde and the lower one is for the lidar. Figure 8 shows the same thing for 20 September 1989, when the inversion was near 200 meters altitude. In this case, both plots show similar ducting conditions. Plots for other days are in the appendix.

CONCLUSIONS

Radio refractivity profiles calculated with the use of lidar data show quite good agreement with those calculated from radiosonde data. Some of the differences observed may be caused by the radiosonde encountering changing atmospheric conditions as it drifts horizontally and rises. In addition, day-to-day changes in the composition of atmospheric aerosols cause some variability in the relationship between the lidar returns and the relative humidity profiles. Calculations of radio refractivity profiles, however, do not appear to be very sensitive to these differences. The strong gradients that occur at the inversion level, in both the lidar return and the relative humidity profile, seem to be the controlling factor in calculating atmospheric ducting and radio-ray coverage. It therefore appears probable that the lidar may be useful for predicting tropospheric ducting of radio waves, and the technique merits further investigation.

RECOMMENDATIONS

The work reported here was accomplished with existing equipment. The lidar was not optimum for this purpose. In addition, the equipment and computer programs were not integrated into a coherent system. To investigate this idea further, we suggest that an "eyesafe" lidar should be obtained. This lidar should have a minimum distance crossover point somewhat less than the 80 to 100 meters of the present lidar. This would allow data to be obtained for elevations closer to the ground.

The lidar should be integrated with a computer, so that the computer controls the firing of the lidar and reads and processes the lidar data. The computer program should provide for the input of ground-based measurements of temperature, pressure, and relative humidity. These would be used as starting points for the standard lapse-rate curves of temperature and pressure. In addition, a ground-based radio refractivity value would be calculated. A linear interpolation between this value and the minimum-altitude lidar value would be used to fill in the lowest few meters of the radio refractivity profile.

The computer should also provide a graphic display for any of the following with just the press of a key: the range-corrected lidar return, the radio refractivity profile calculated from the lidar data, and the predicted radio-ray coverage. The system should also be capable of providing a hard copy of any of these graphs.

This system should be tested in a variety of locations and weather conditions.

REFERENCES

Fitzgerald, James W. 1984. "Effect of Relative Humidity on the Aerosol Backscattering Coefficient at 0.694 and 10.6 m Wavelengths." *Applied Optics*, vol. 23, no. 3, pp. 411-418.

Hitney, H. V., A. E. Barrios, and G. E. Lindem. 1988. "Engineer's Refractive Effects Prediction System (EREPS)." NOSC TD 1342 (July). Naval Ocean Systems Center, San Diego, CA.

Lentz, W. J. 1982. "The Visioceilometer: A Portable Visibility and Cloud Ceiling Height Lidar." ASL TR 0105 (January). Atmospheric Sciences Laboratory, White Sands Missile Range, NM.

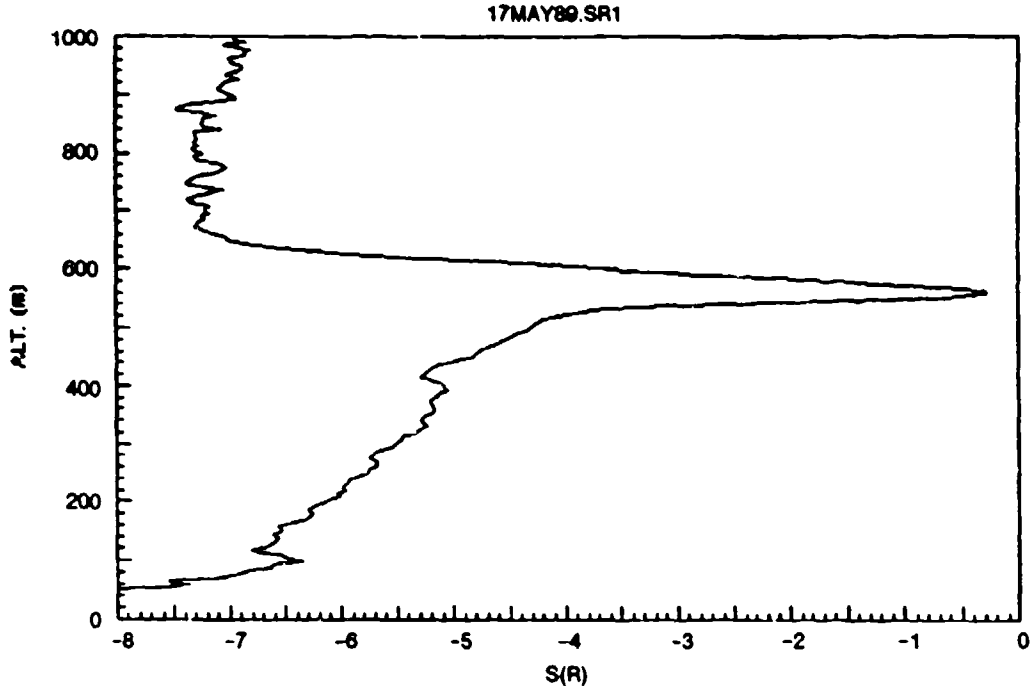

Figure 1. Example of a range-compensated lidar return from a cloud.

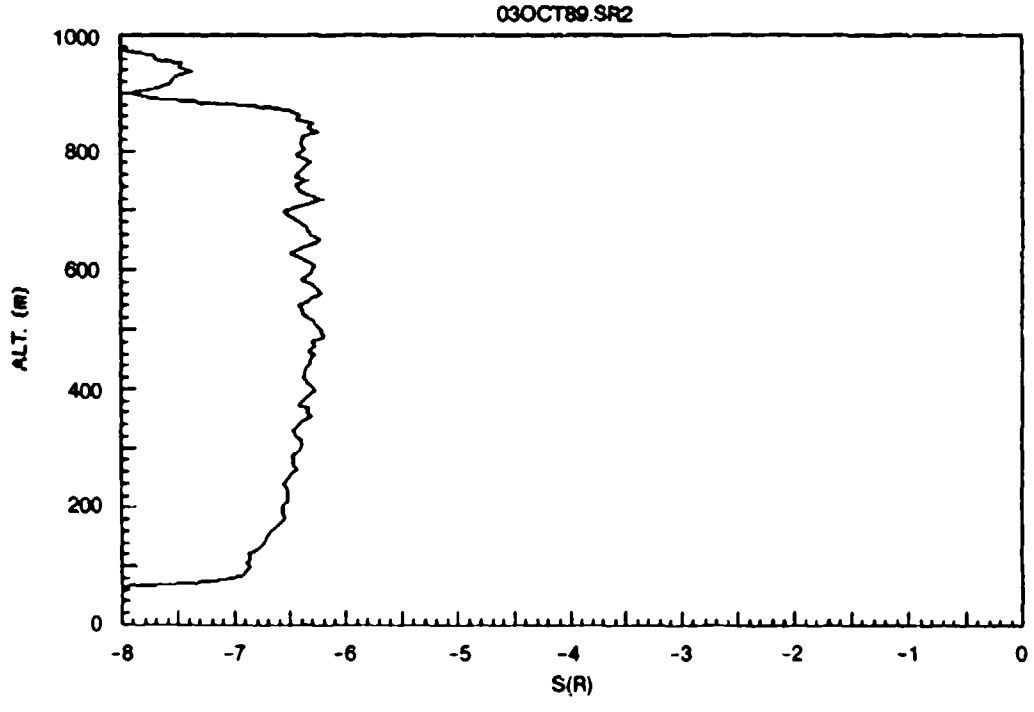

Figure 2. Example of a vertical range-compensated lidar return in the presence of an inversion. Plotted on the same scale as figure 1 for comparison.

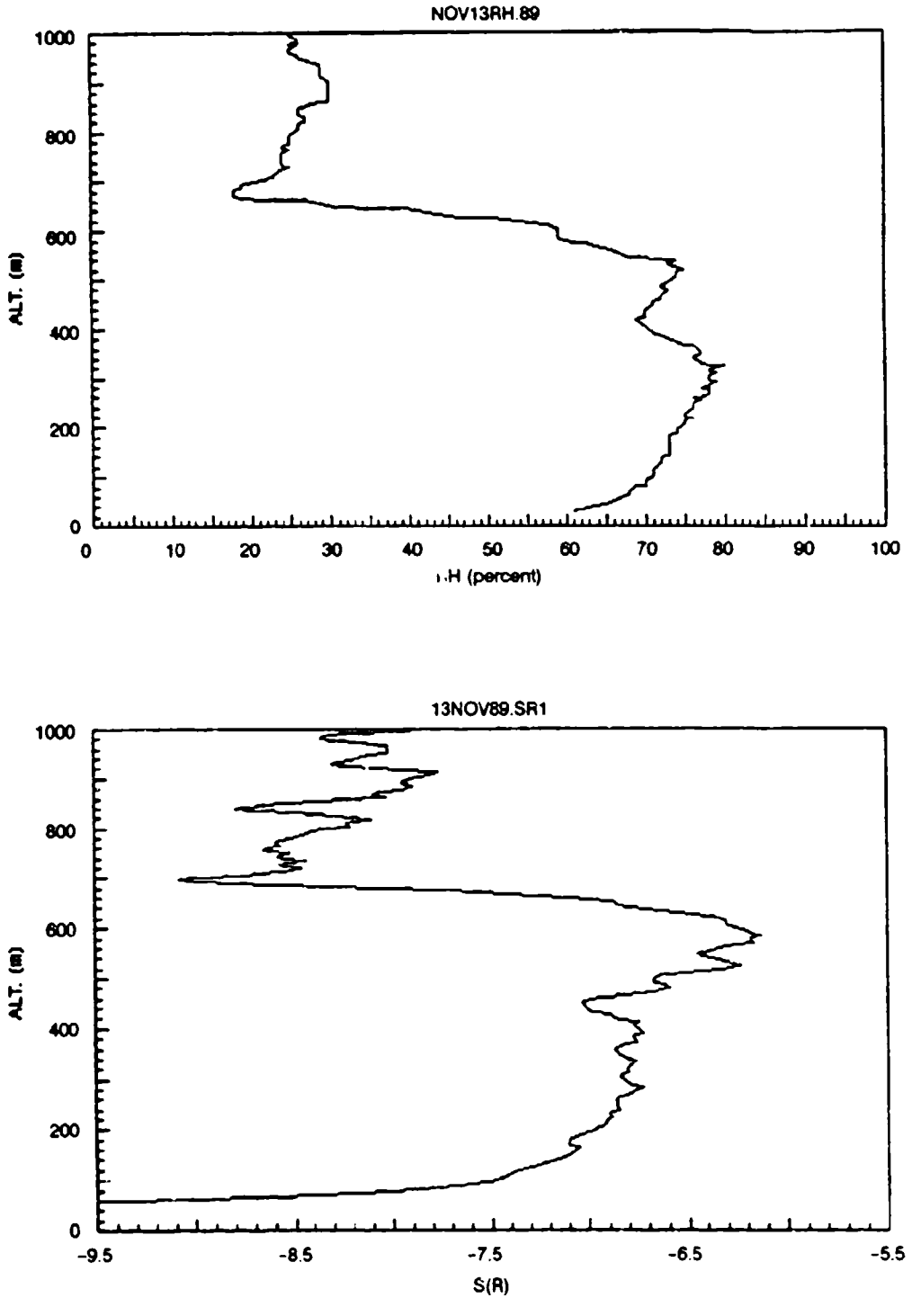

Figure 3. An example comparing the range-corrected lidar return with a relative humidity profile taken at the same time. The upper curve is for the relative humidity.

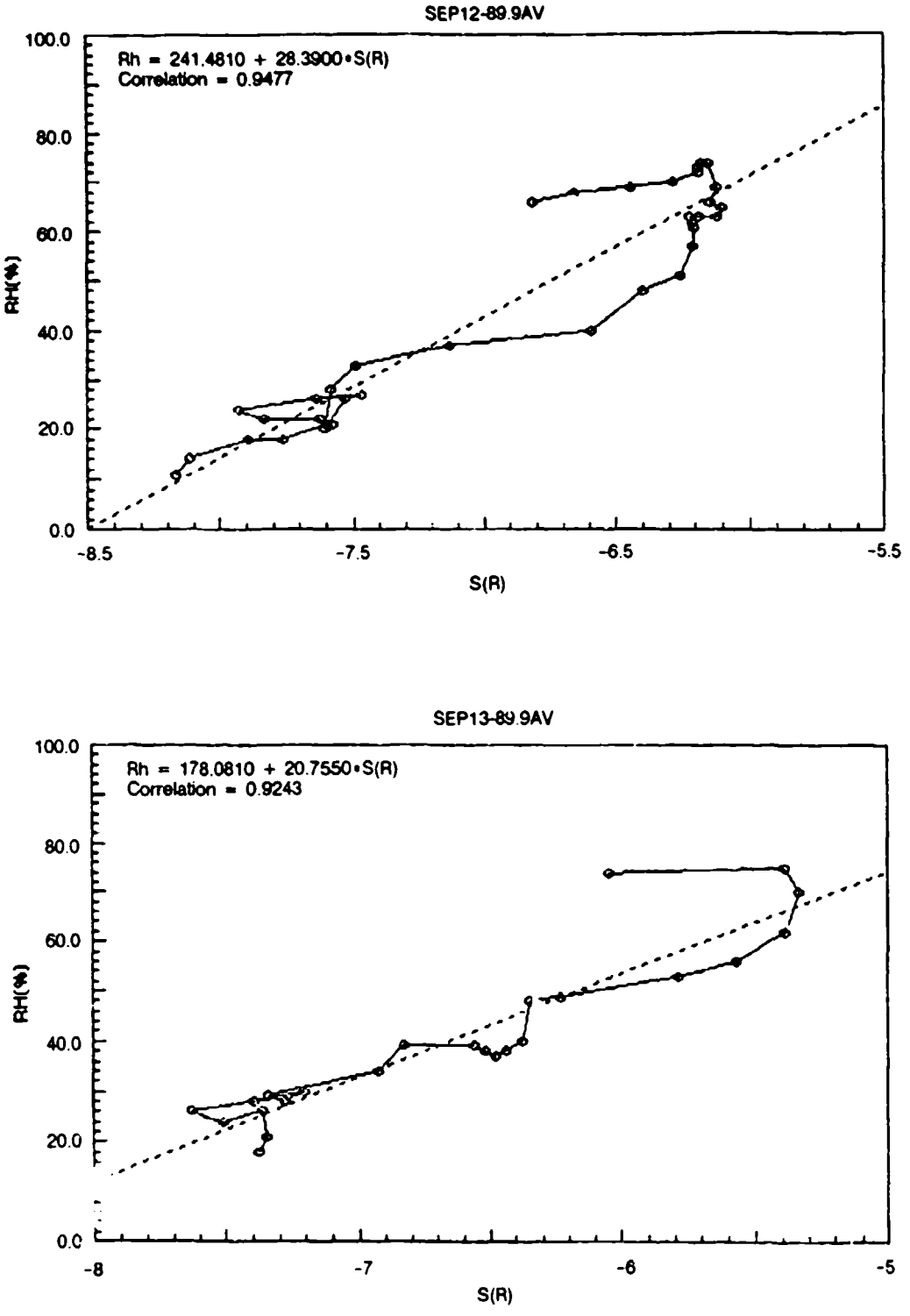

Figure 4. Plots of relative humidity as a function of range-compensated lidar return, S(R).

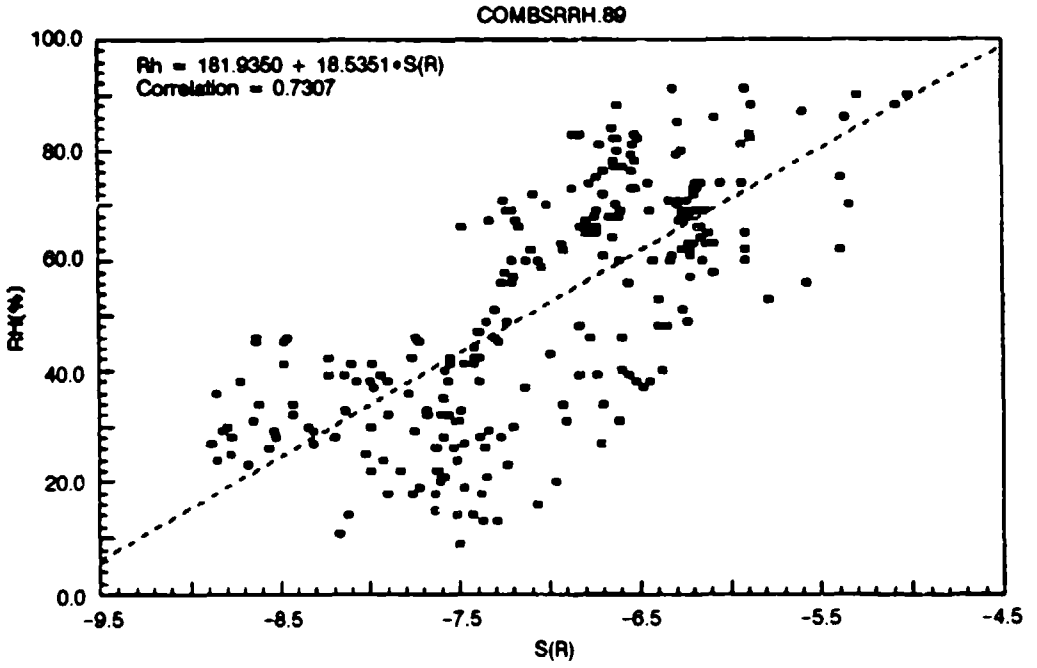

Figure 5. Relative humidity plotted as a function of range-compensated lidar return, S(R), for all of the data samples.

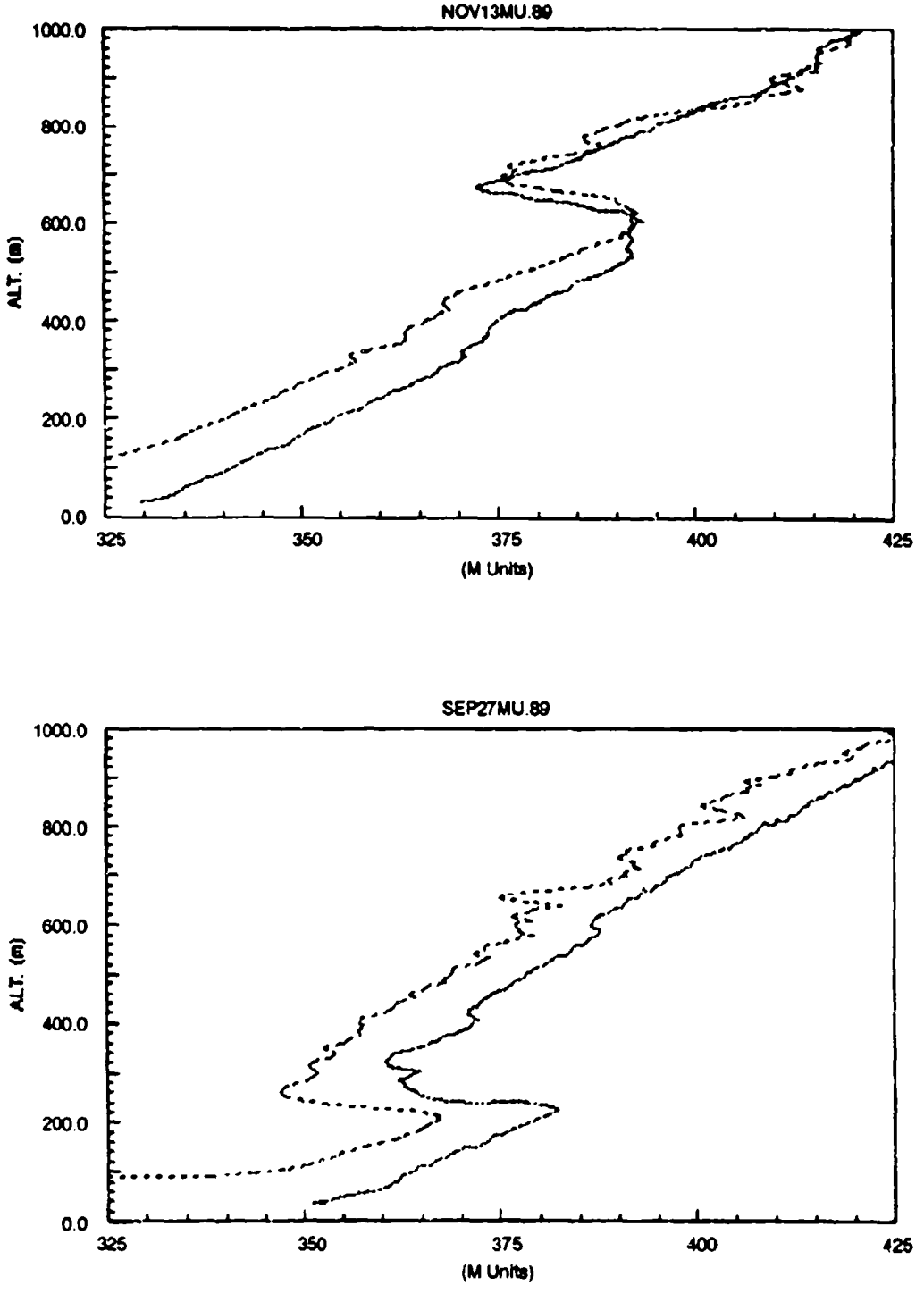

Figure 6. Two examples comparing radio refractivity M-unit profiles calculated with lidar data with corresponding profiles calculated with radiosonde data. The dashed curves are for the lidar data.

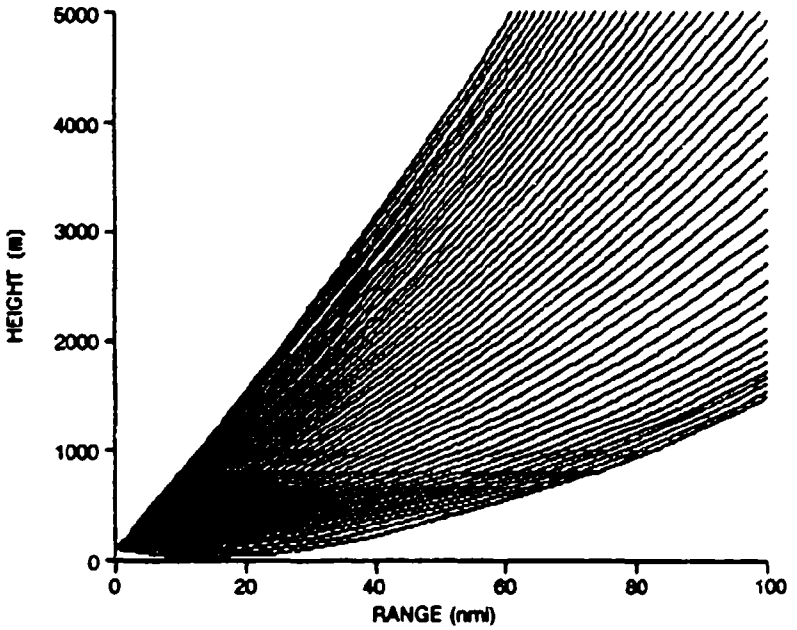

ANT HT m	100
# of RAYS	50
MIN ANG mrad	-4.9
MAX ANG mrad	37.5
REFLECTED RAYS	Y

PROFILE

HEIGHT(m)	M-UNITS
0.0	330.0
200.3	365.0
301.5	370.5
405.4	376.8
479.5	384.3
593.9	387.5
611.1	383.5
683.9	377.0
782.2	395.3
815.3	398.4
859.0	400.7
930.8	408.7
1006.9	418.5

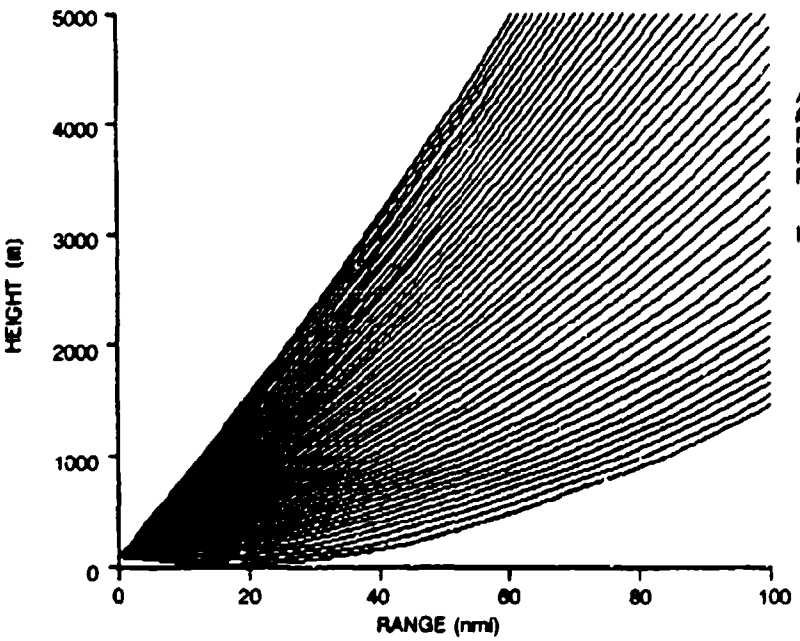

ANT HT m	100
# of RAYS	50
MIN ANG mrad	-4.9
MAX ANG mrad	37.5
REFLECTED RAYS	Y

PROFILE

HEIGHT(m)	M-UNITS
0.0	325.0
202.5	355.0
300.0	368.0
405.0	376.1
480.0	384.8
592.5	401.8
630.0	388.0
660.0	380.5
675.0	379.7
780.0	399.7
817.5	385.4
855.0	406.0
930.0	413.7
1005.0	421.3

Figure 7. Radio-ray coverage predictions for an inversion near 600 meters altitude, which occurred on 12 September 1989. Upper curve is for radiosonde data and lower curve is for lidar data.

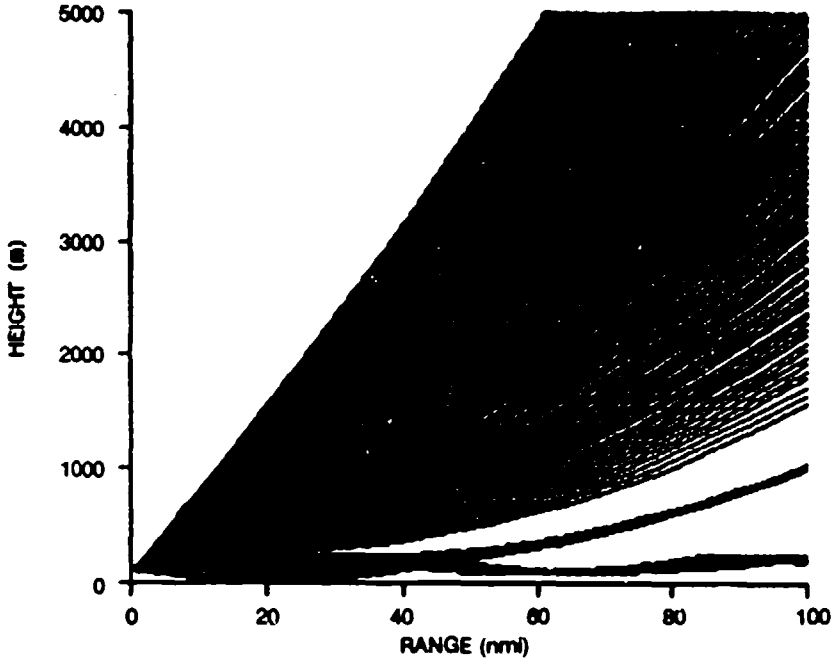

ANT HT m	100
# of RAYS	200
MIN ANG mrad	-4.8
MAX ANG mrad	37.5
REFLECTED RAYS	Y

PROFILE

HEIGHT(m)	M-UNITS
0.0	330.0
149.5	349.5
222.1	356.3
259.5	340.5
275.2	346.6
311.1	343.2
364.9	354.9
499.7	362.2
600.5	372.9
699.9	382.7
798.4	396.2
899.0	407.1
1007.4	422.7

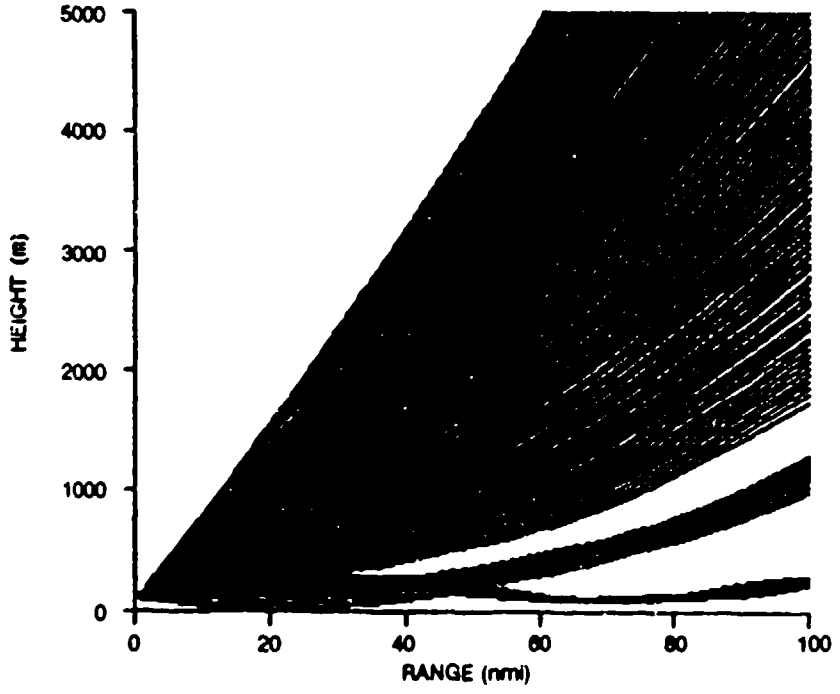

ANT HT m	100
# of RAYS	200
MIN ANG mrad	-4.9
MAX ANG mrad	37.5
REFLECTED RAYS	Y

PROFILE

HEIGHT(m)	M-UNITS
0.0	315.0
150.0	332.4
225.0	345.4
285.0	325.7
307.5	357.2
337.5	327.9
375.0	348.9
412.5	352.7
480.0	348.6
517.5	356.5
600.0	344.6
705.0	376.7
810.0	390.0
900.0	396.0
1005.0	419.4

Figure 8. Radio-ray coverage predictions for an inversion near 200 meters altitude, which occurred on 20 September 1989. Upper curve is for radiosonde data and lower curve is for lidar data.

APPENDIX

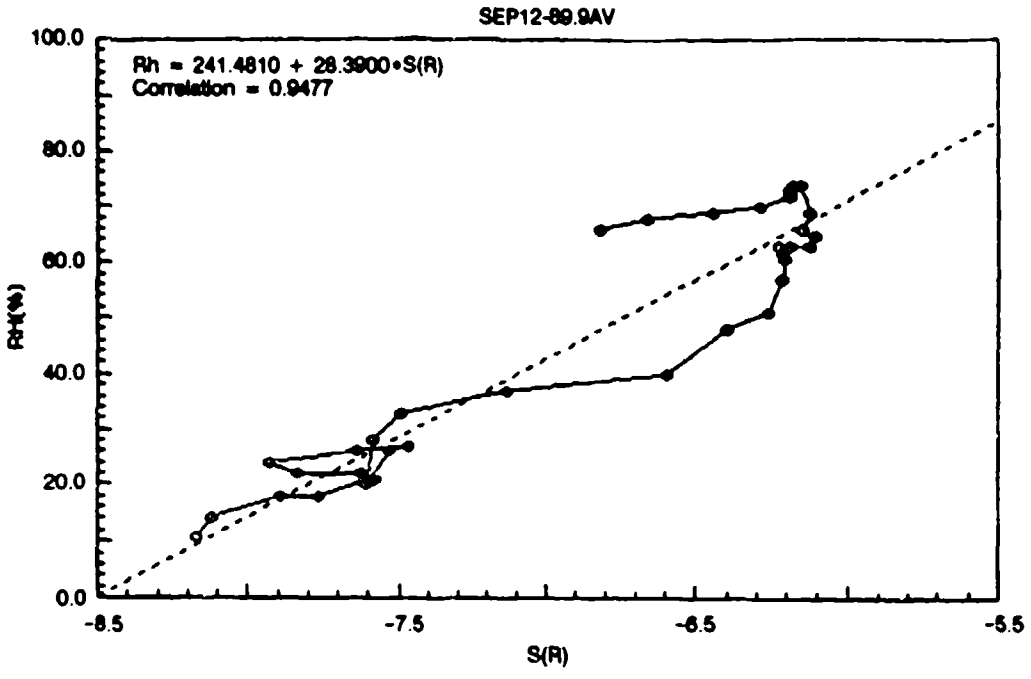

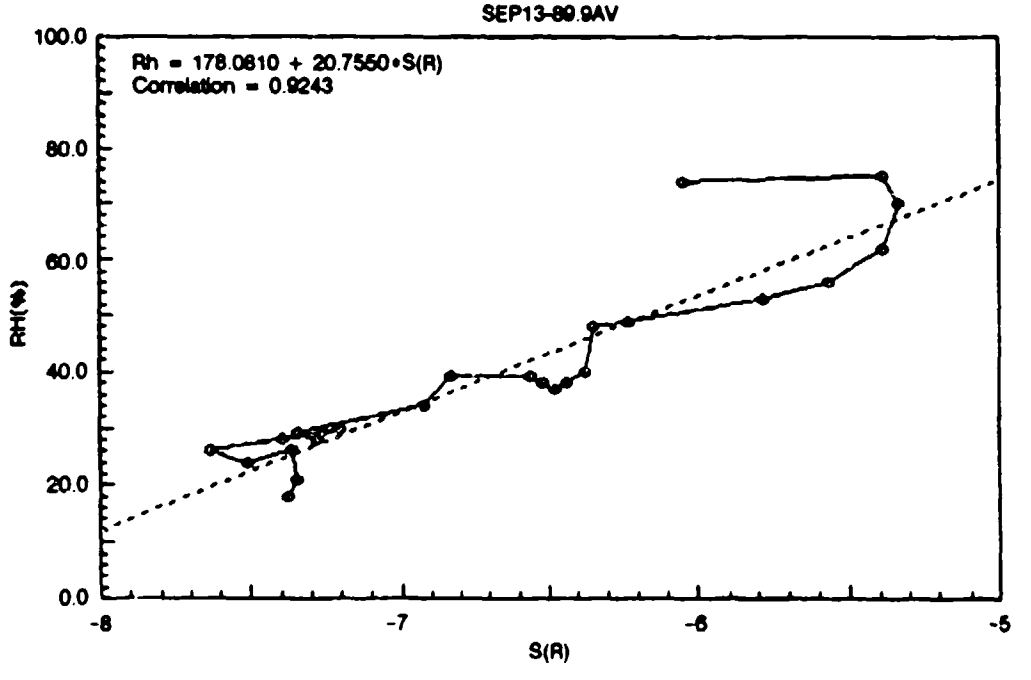

Figure A1. Plots of relative humidity as a function of lidar S(R) returns.

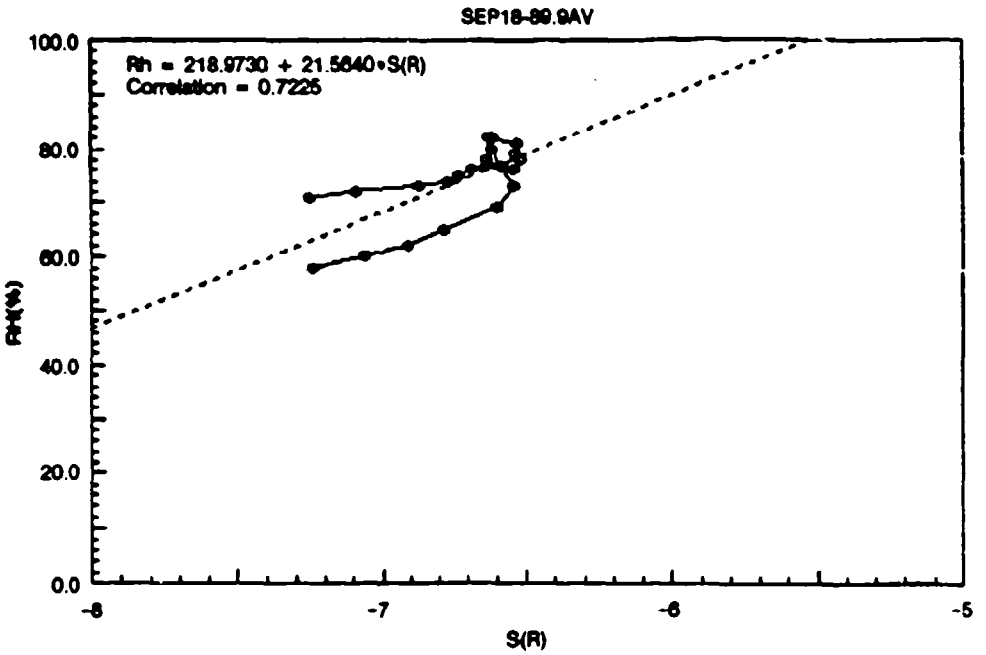

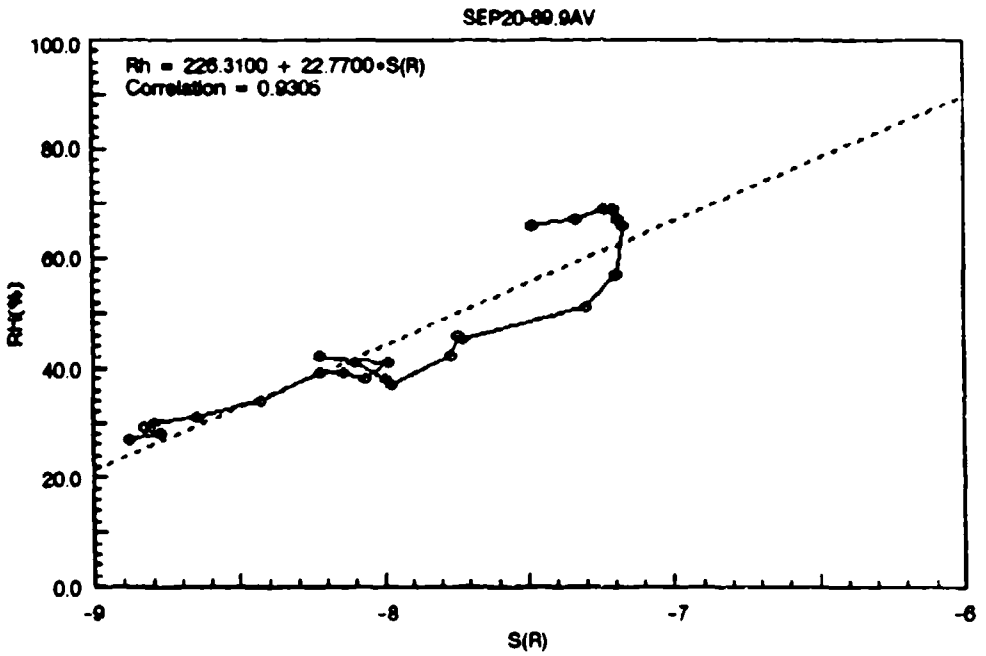

Figure A1. (Continued.)

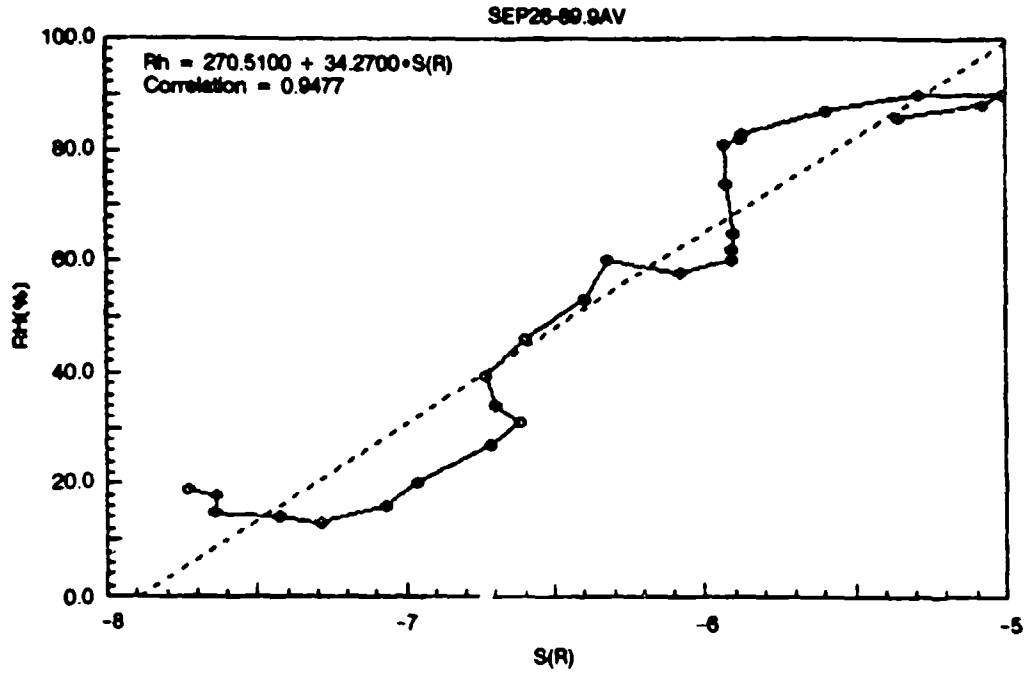

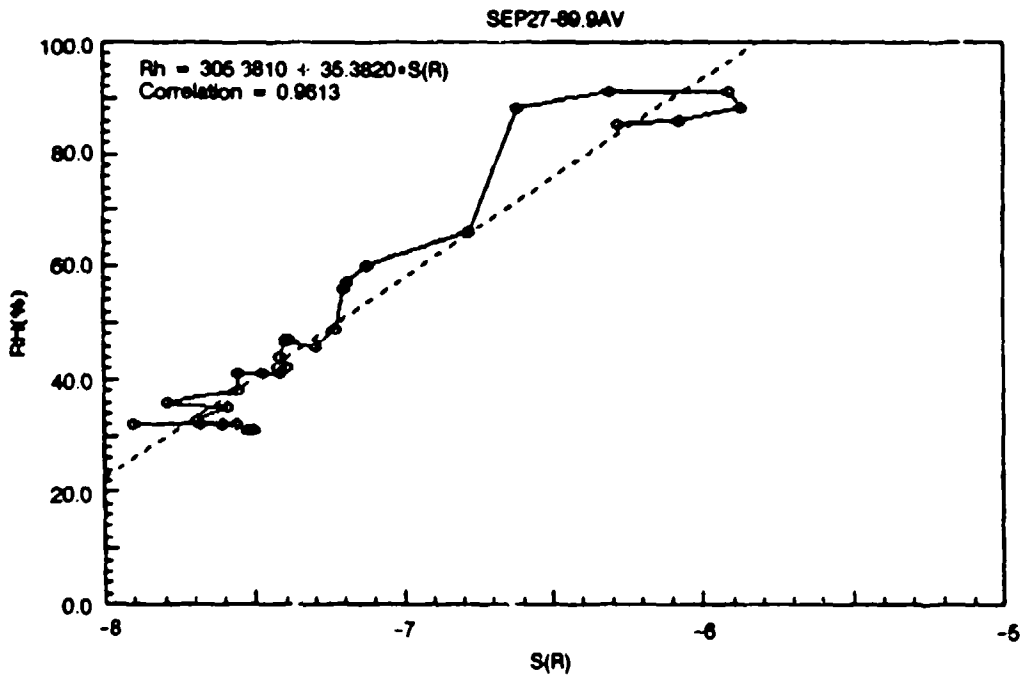

Figure A1. (Continued.)

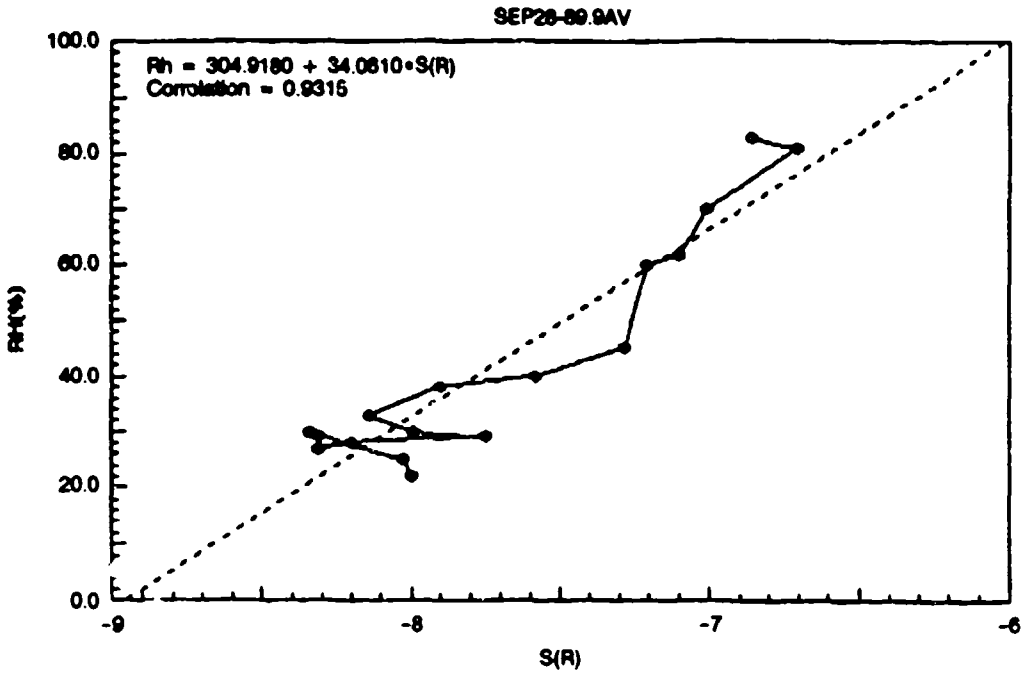

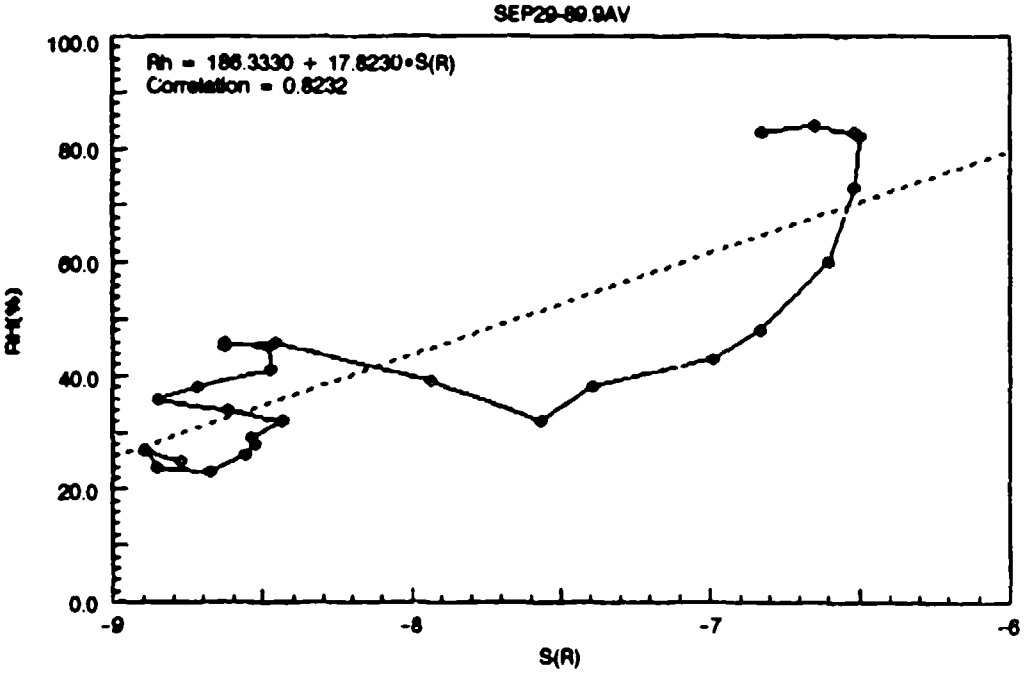

Figure A1. (Continued.)

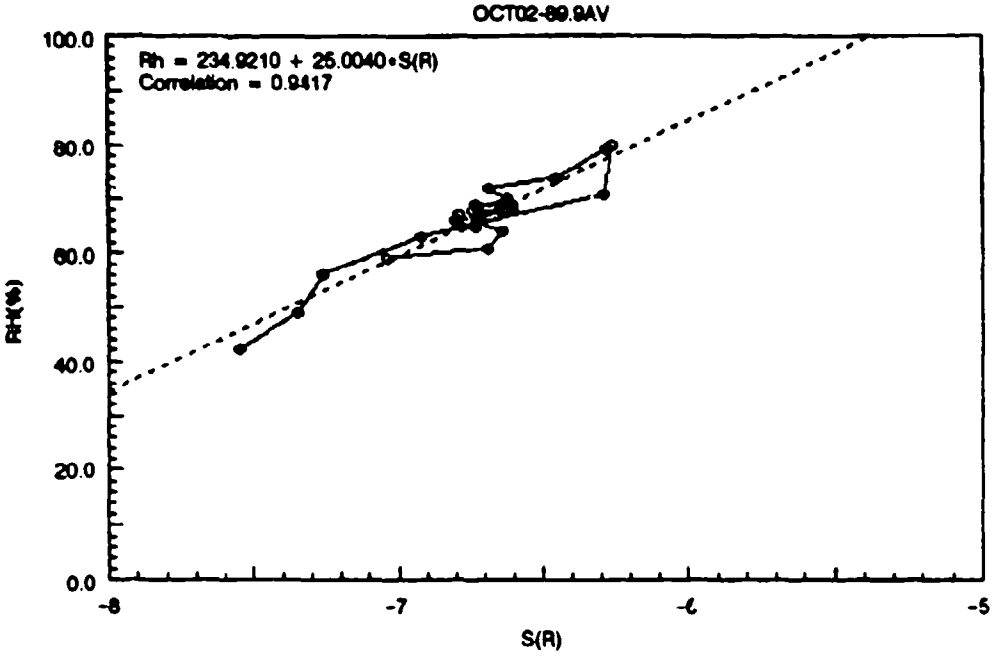

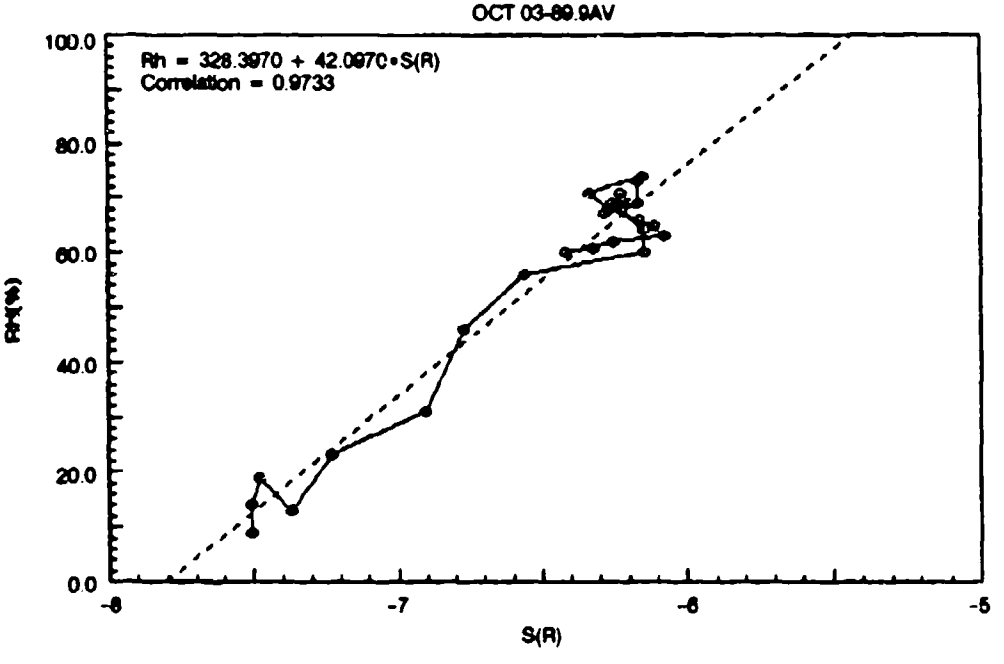

Figure A1. (Continued.)

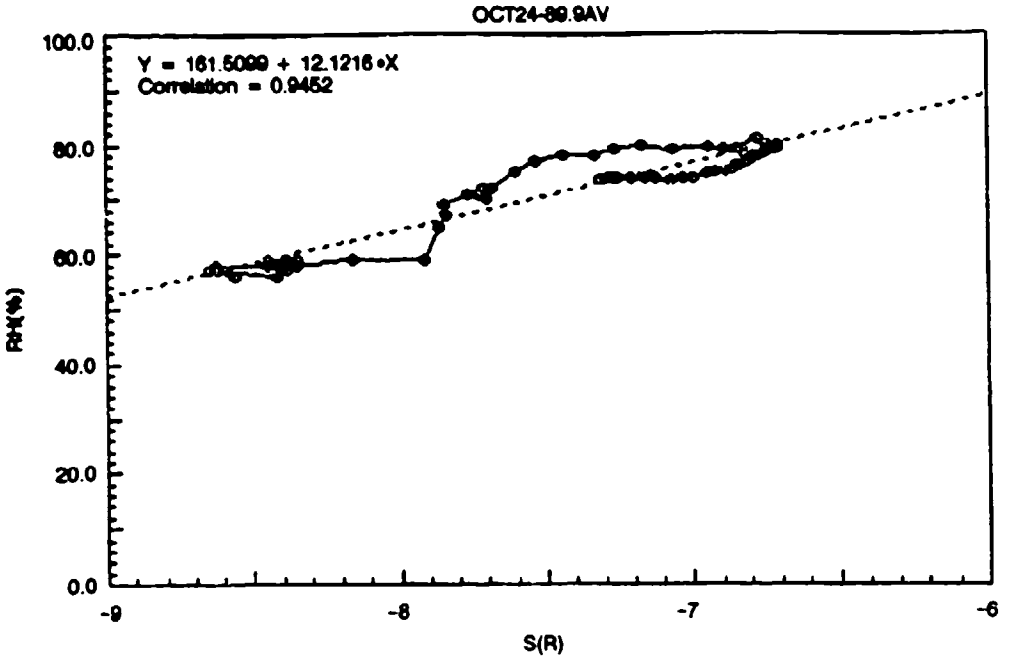

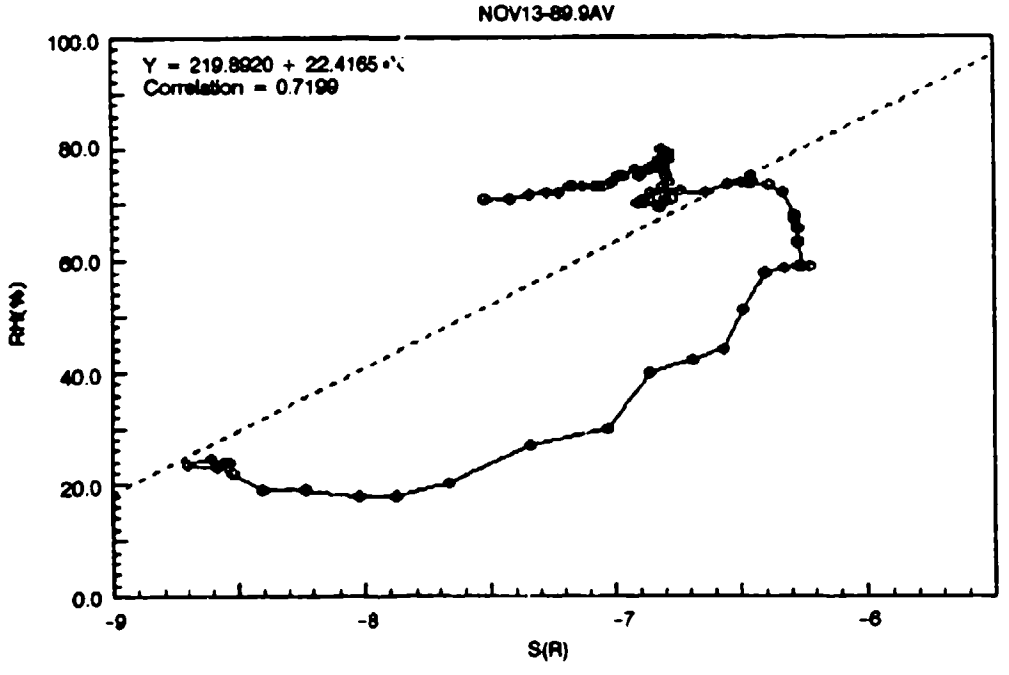

Figure A1. (Continued.)

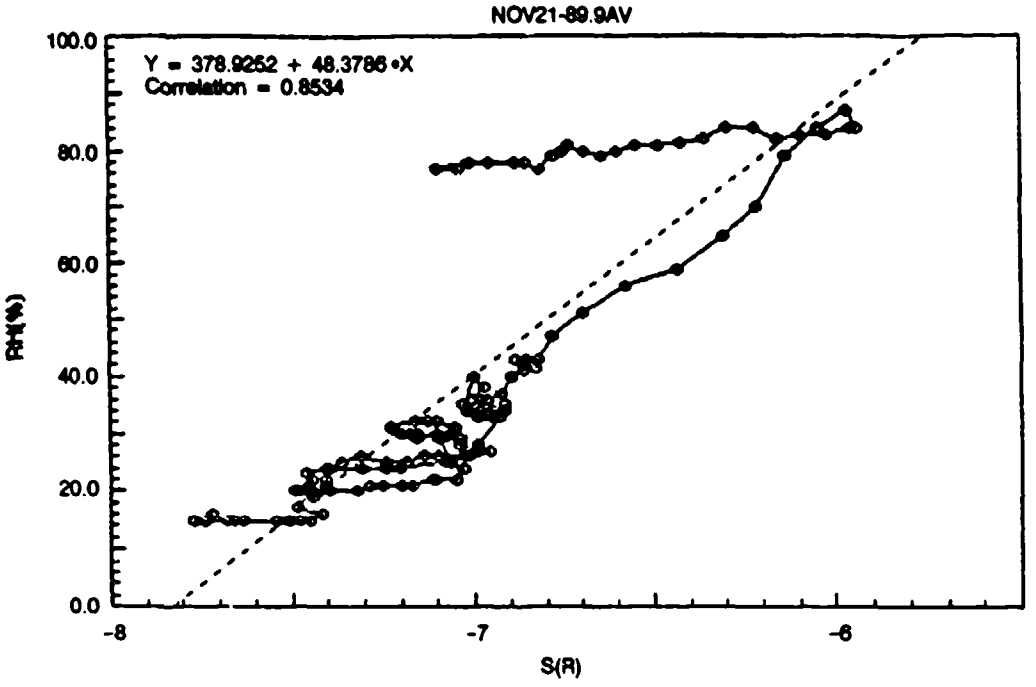

Figure A1. (Continued.)

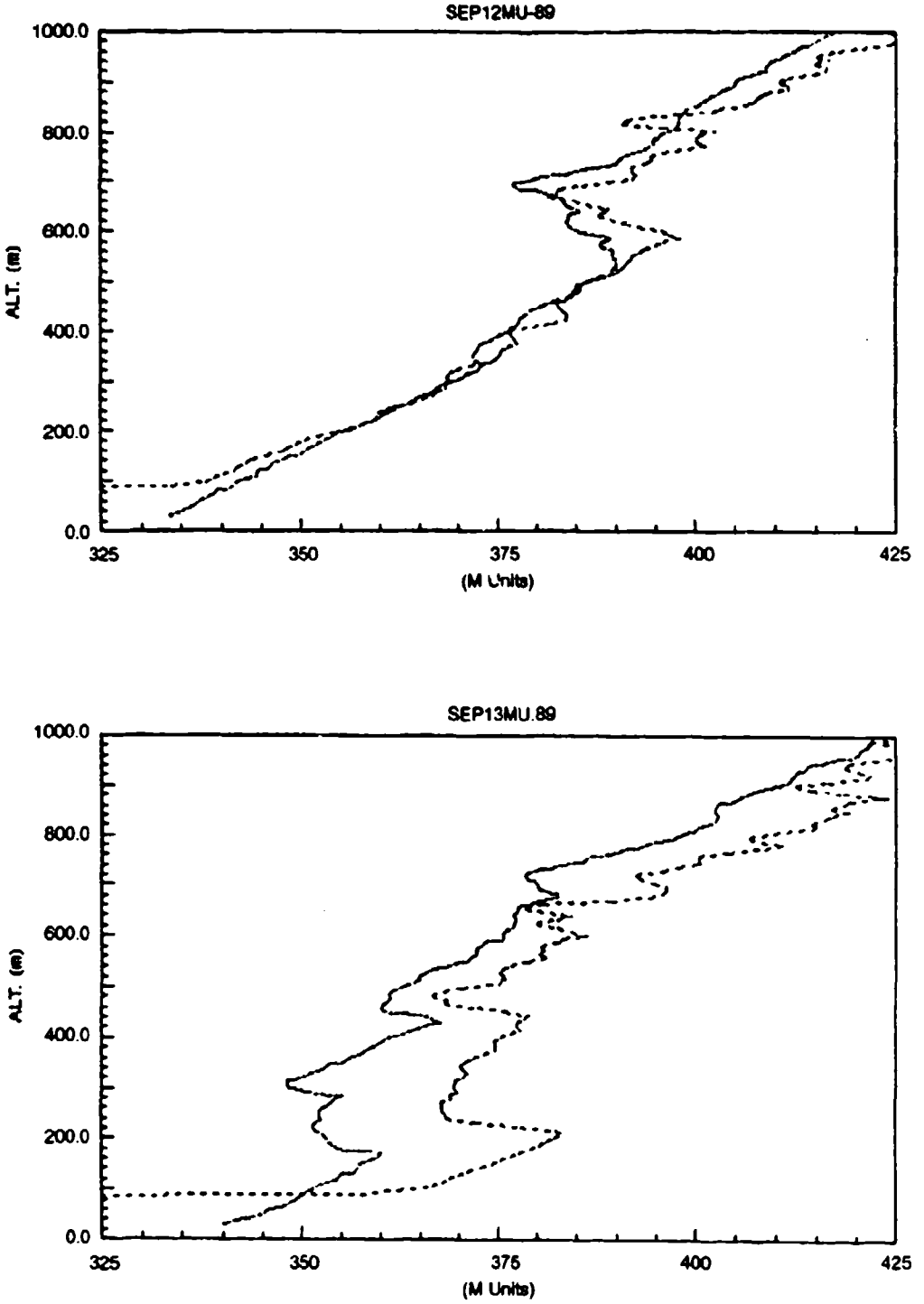

Figure A2. Comparison of radio-refractivity profiles calculated with the use of lidar data with those calculated from radiosonde data. Dashed curves are from the lidar data.

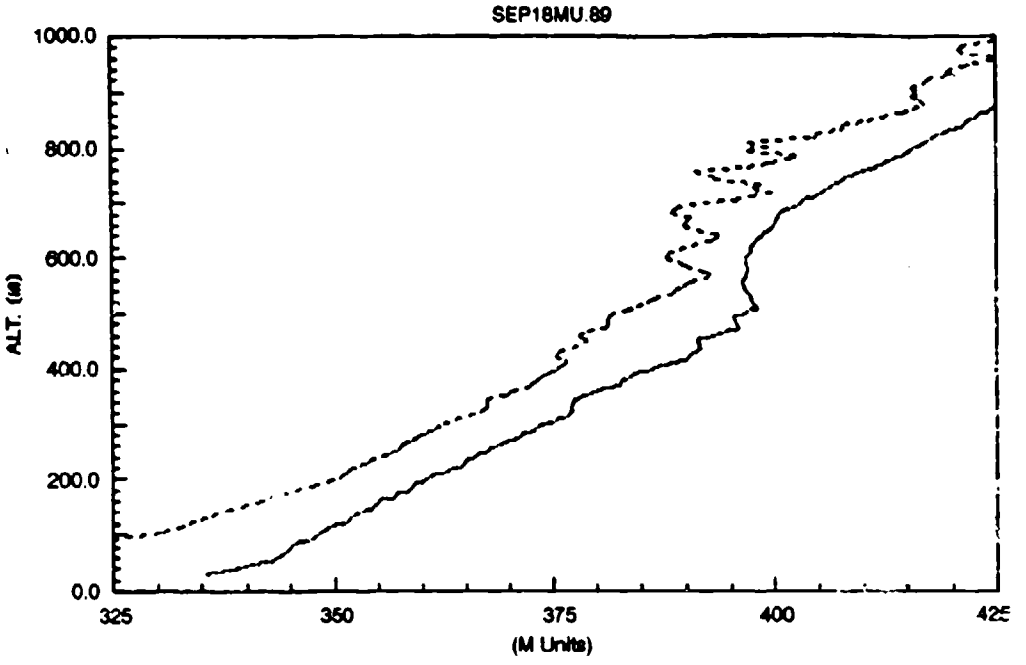

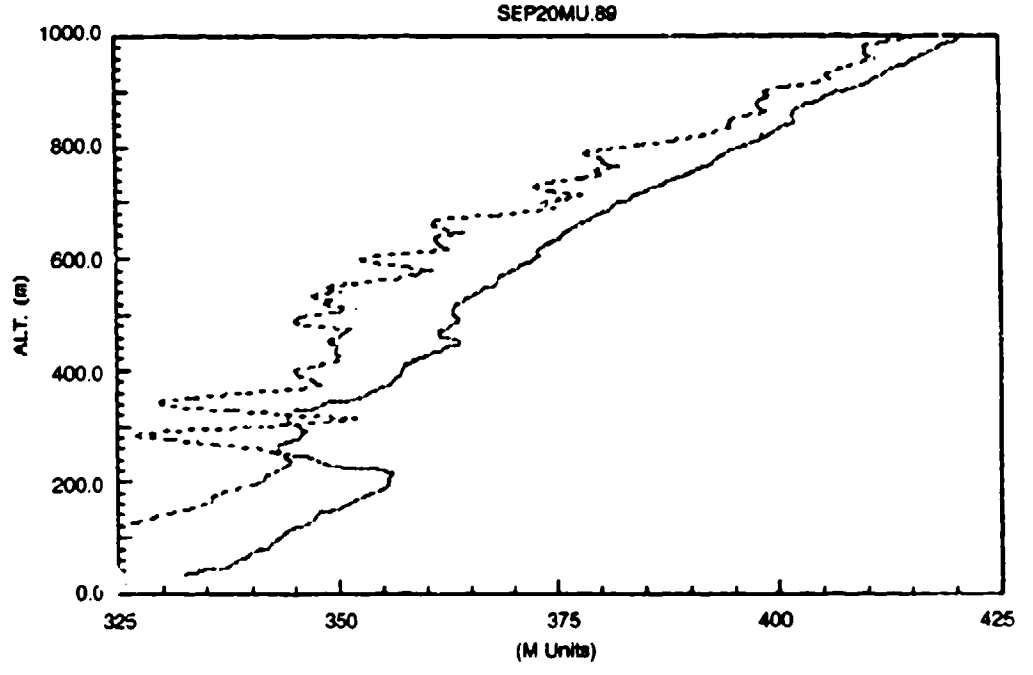

Figure A2. (Continued.)

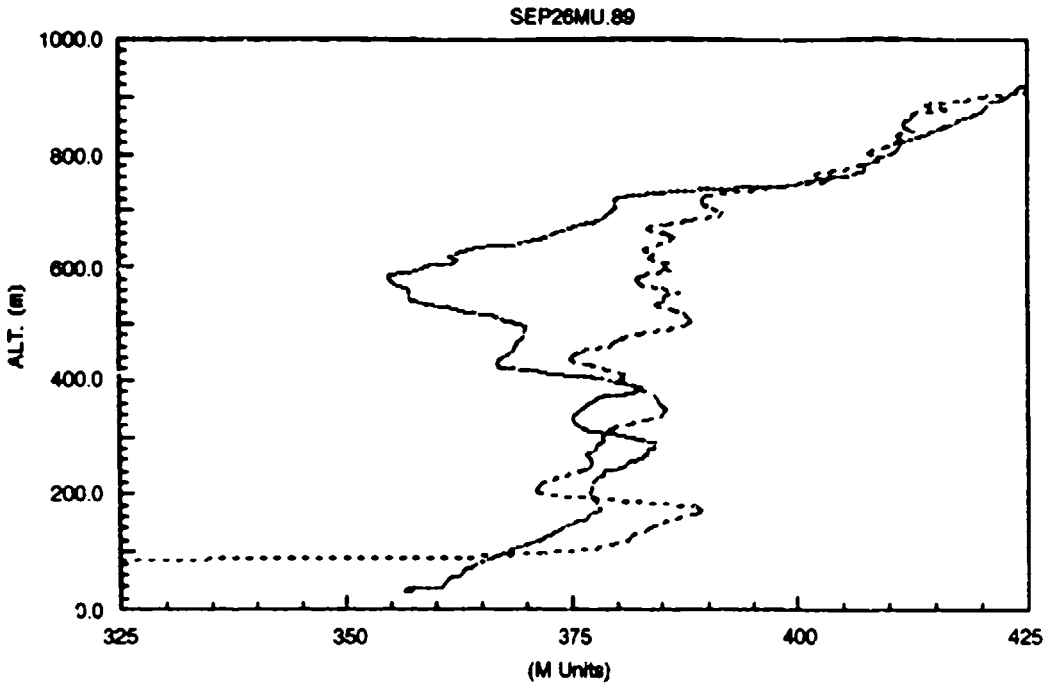

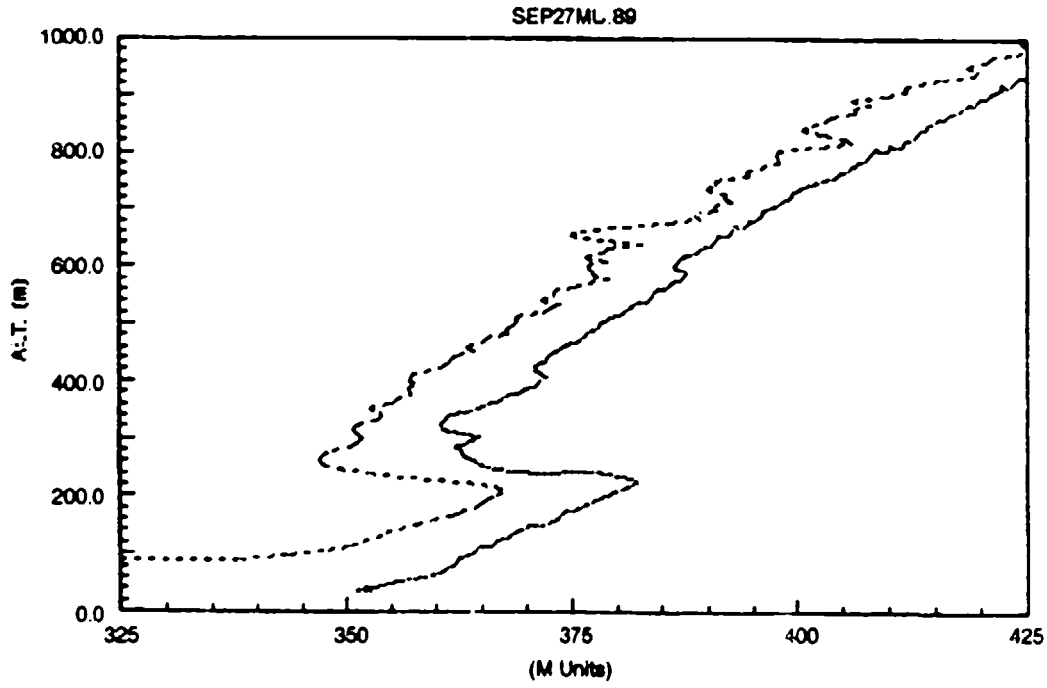

Figure A2. (Continued.)

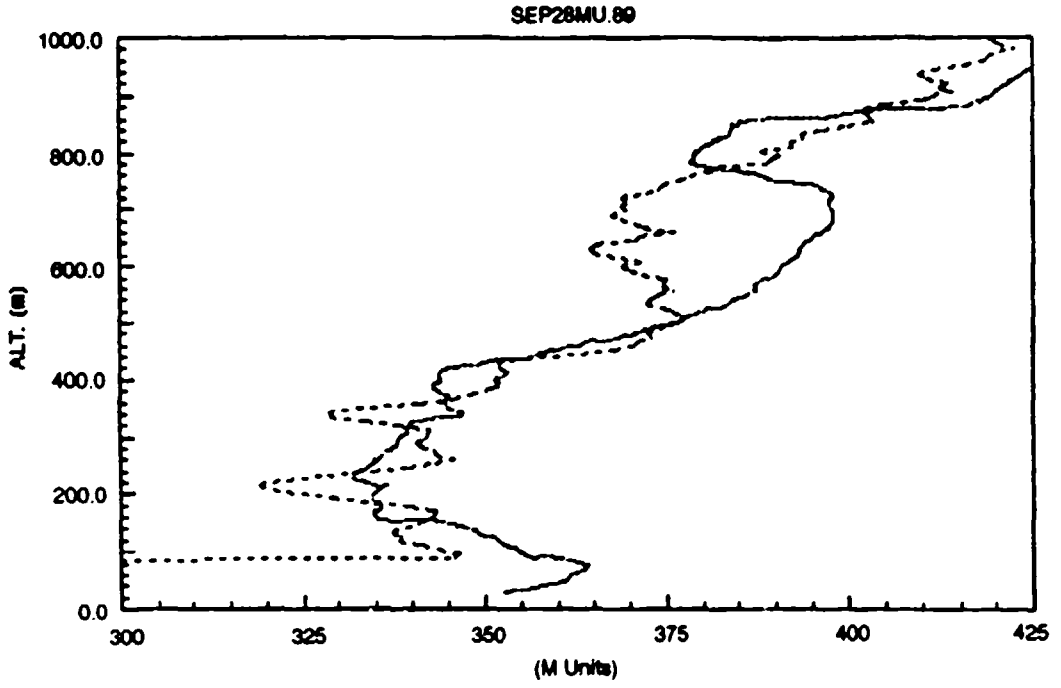

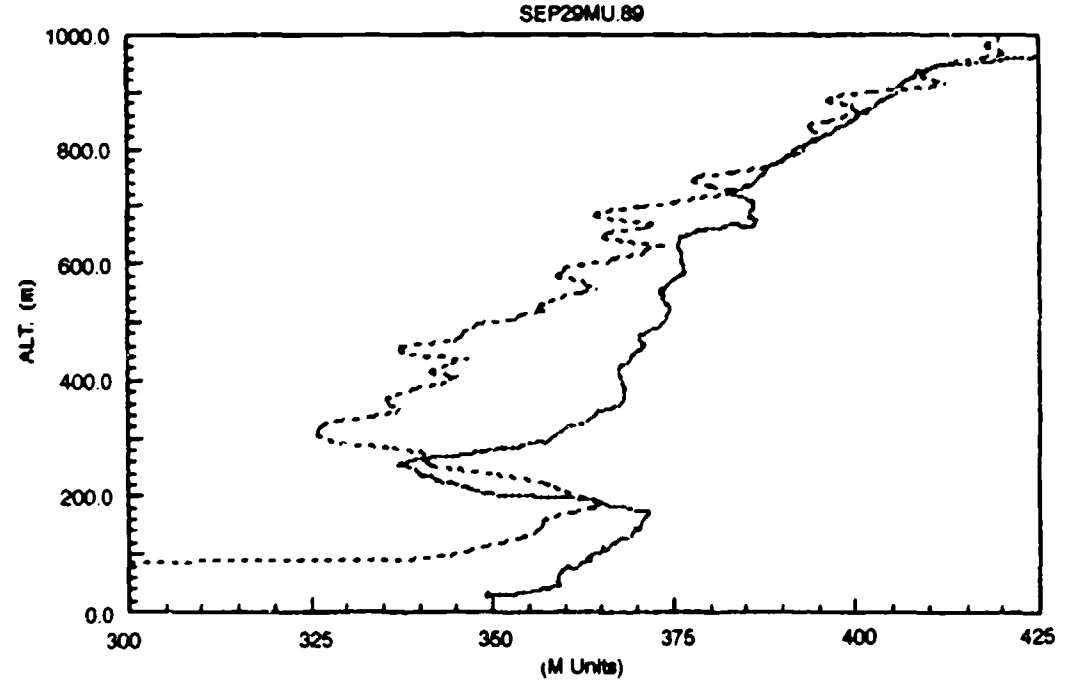

Figure A2. (Continued.)

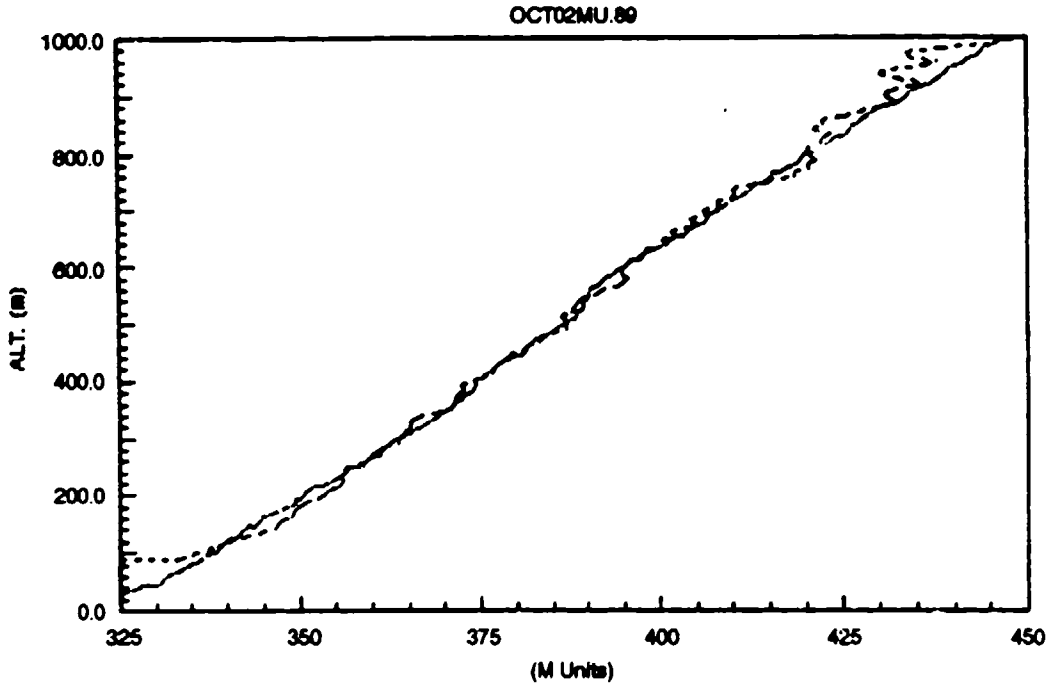

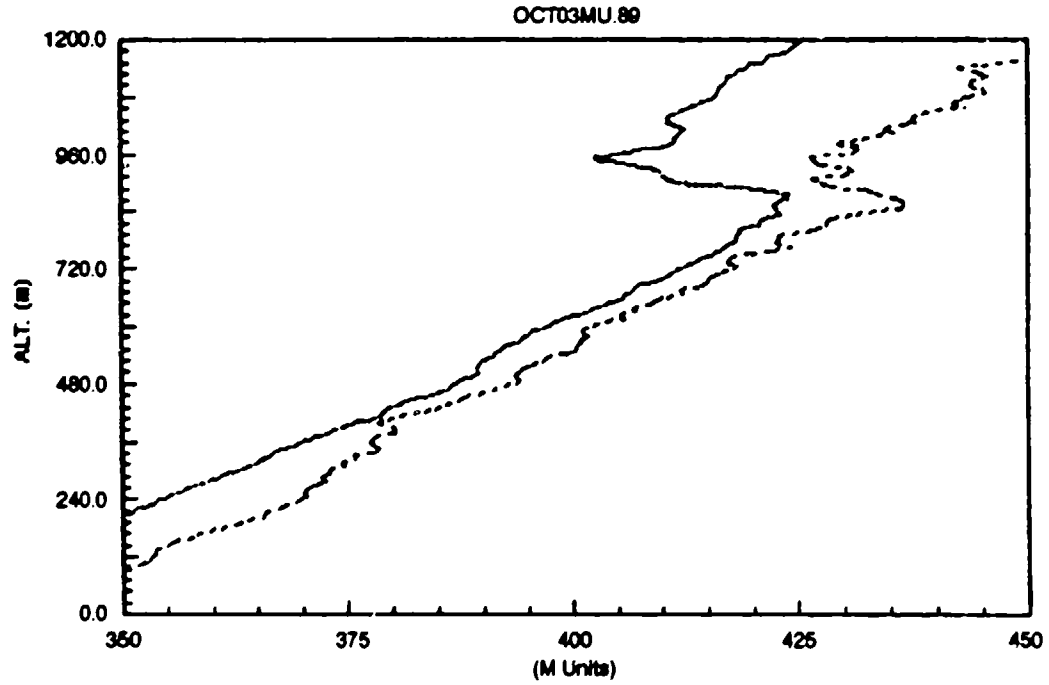

Figure A2. (Continued.)

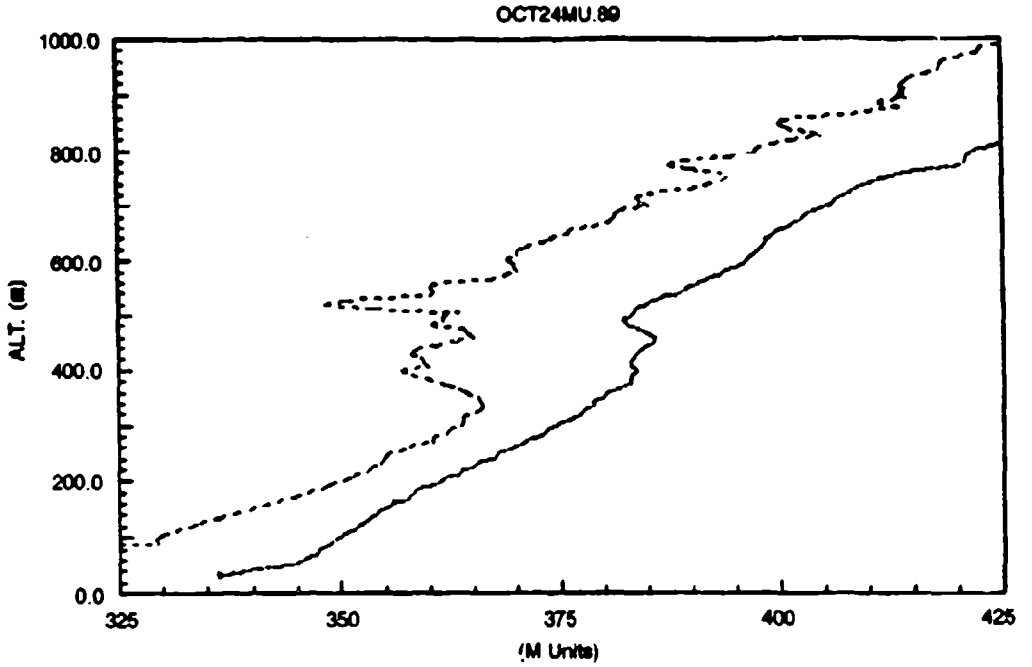

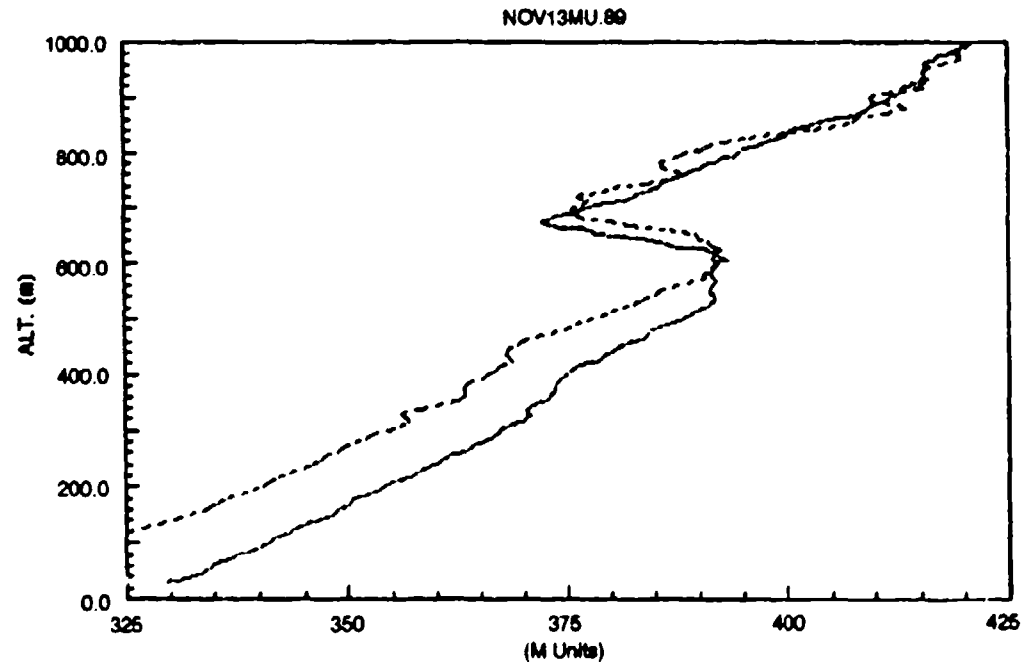

Figure A2. (Continued.)

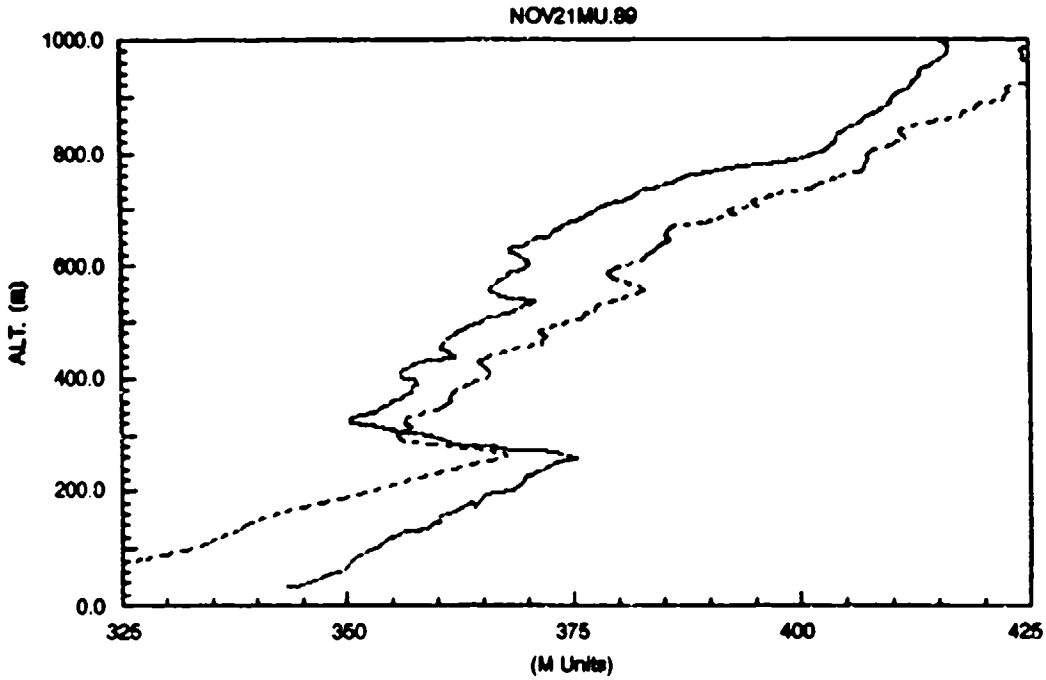

Figure A2. (Continued.)

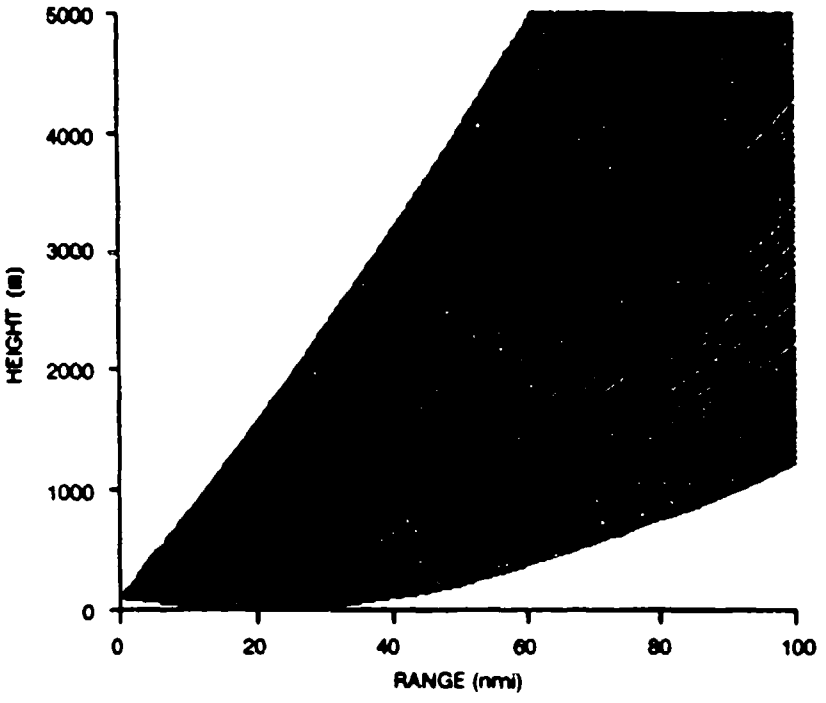

ANT HT m	100
# of RAYS	200
MIN ANG mrad	-4.9
MAX ANG mrad	37.5
REFLECTED RAYS	Y

PROFILE

HEIGHT(m)	M-UNITS
0.0	330.0
200.3	356.0
301.5	370.5
403.7	376.6
501.9	387.8
583.0	389.5
635.9	385.0
693.2	376.2
748.3	390.7
804.0	397.0
899.2	405.9
951.0	411.3
1006.9	418.5

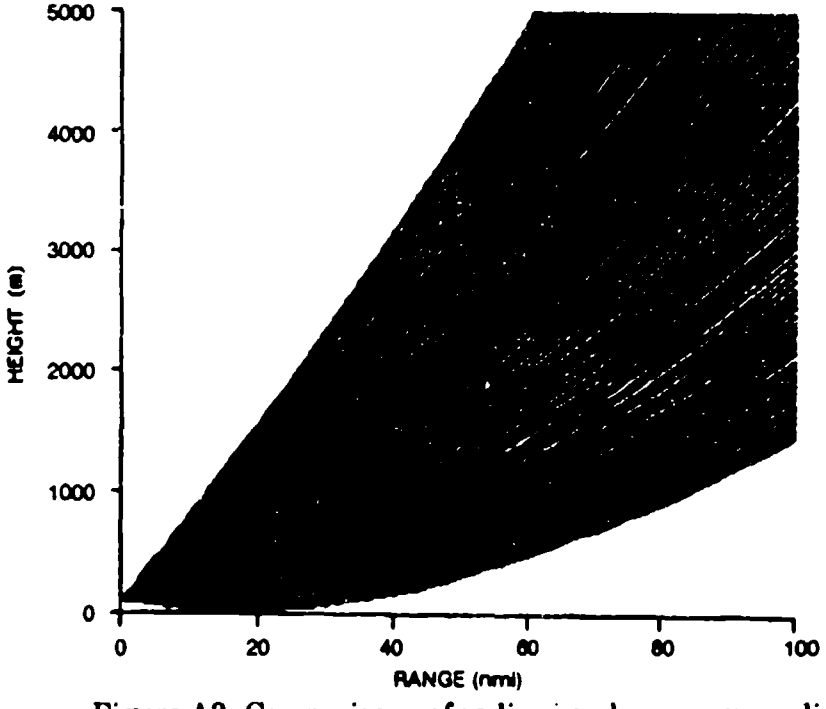

ANT HT m	100
# of RAYS	200
MIN ANG mrad	-4.9
MAX ANG mrad	37.5
REFLECTED RAYS	Y

PROFILE

HEIGHT(m)	M-UNITS
0.0	325.0
202.5	355.7
300.0	368.0
405.0	378.1
502.5	388.0
592.5	401.8
622.5	386.8
660.0	380.5
675.0	379.4
705.0	393.9
802.5	401.3
900.0	407.5
952.5	418.9
1005.0	421.3

Figure A3. Comparisons of radio-signal coverage predicted with the use of lidar data with that from radiosonde data. Upper graph is for radiosonde data. Data for 12 September 1989.

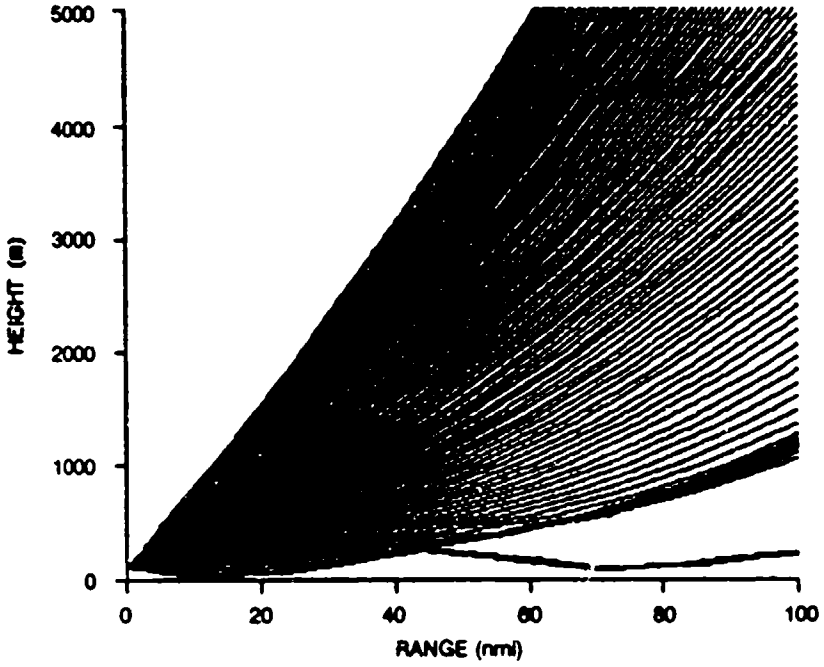

ANT HT m	100
# of RAYS	100
MIN ANG mrad	-4.9
MAX ANG mrad	37.5
REFLECTED RAYS	Y

PROFILE

HEIGHT(m)	M-UNITS
0.0	330.0
176.7	360.6
223.7	350.3
259.0	353.0
283.8	355.1
301.5	347.2
401.3	361.5
429.3	367.5
458.4	359.7
500.3	362.8
558.2	372.9
637.8	377.1
709.8	380.2
801.4	398.7
1005.5	422.3

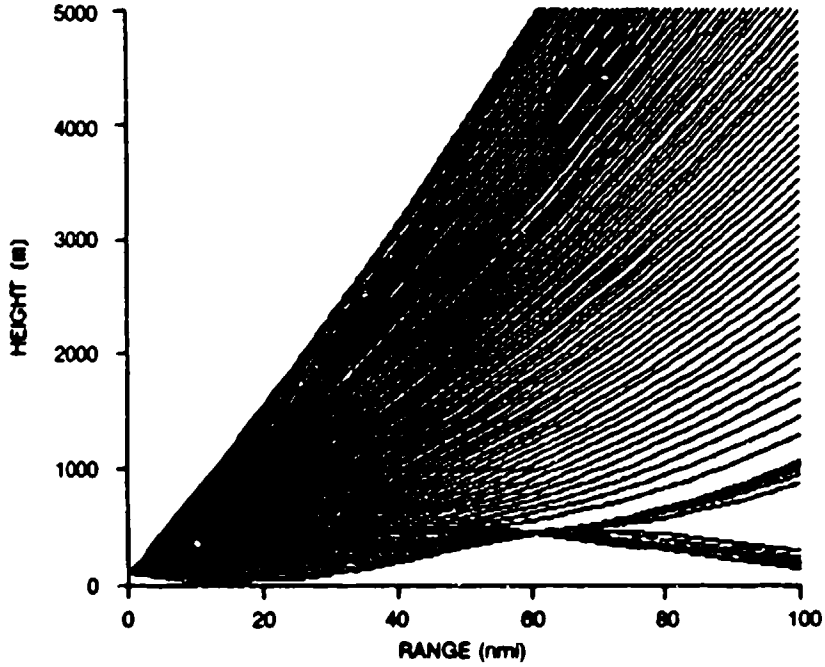

ANT HT m	100
# of RAYS	100
MIN ANG mrad	-4.9
MAX ANG mrad	37.5
REFLECTED RAYS	Y

PROFILE

HEIGHT(m)	M-UNITS
0.0	350.0
217.5	385.4
315.0	367.5
442.5	380.7
472.5	365.5
487.5	364.0
517.5	371.5
577.5	383.0
637.5	387.4
720.0	393.4
825.0	418.6
900.0	407.8
960.0	427.3
1005.0	435.6

Figure A3. (Continued.) Data for 13 September 1989.

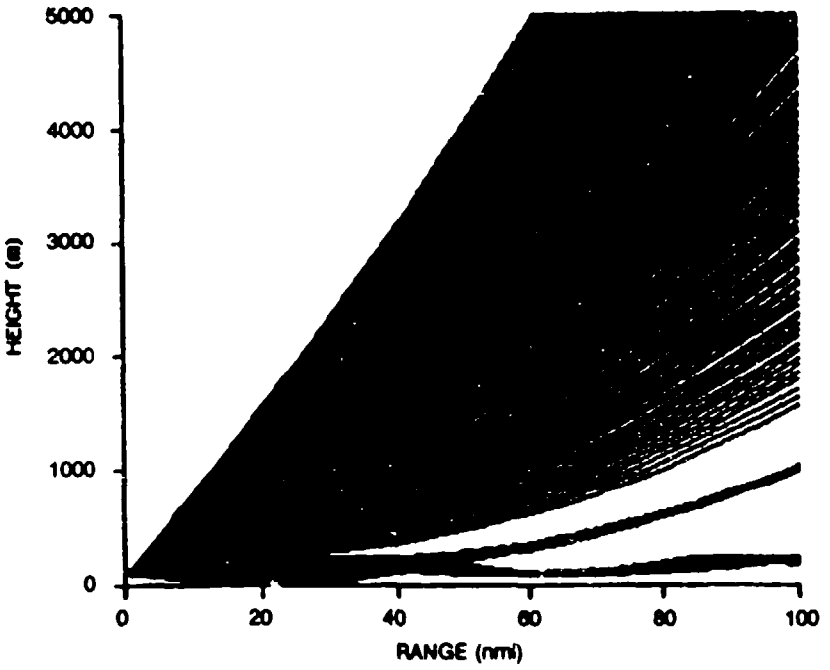

ANT HT m	100
# of RAYS	200
MIN ANG mrad	-4.9
MAX ANG mrad	37.5
REFLECTED RAYS	Y

PROFILE

HEIGHT (m)	M-UNITS
0.0	330.0
149.5	349.5
222.1	356.3
259.5	340.5
275.2	346.6
311.1	343.2
364.9	354.9
499.7	362.2
600.5	372.9
699.9	382.7
798.4	396.2
899.0	407.1
1007.4	422.7

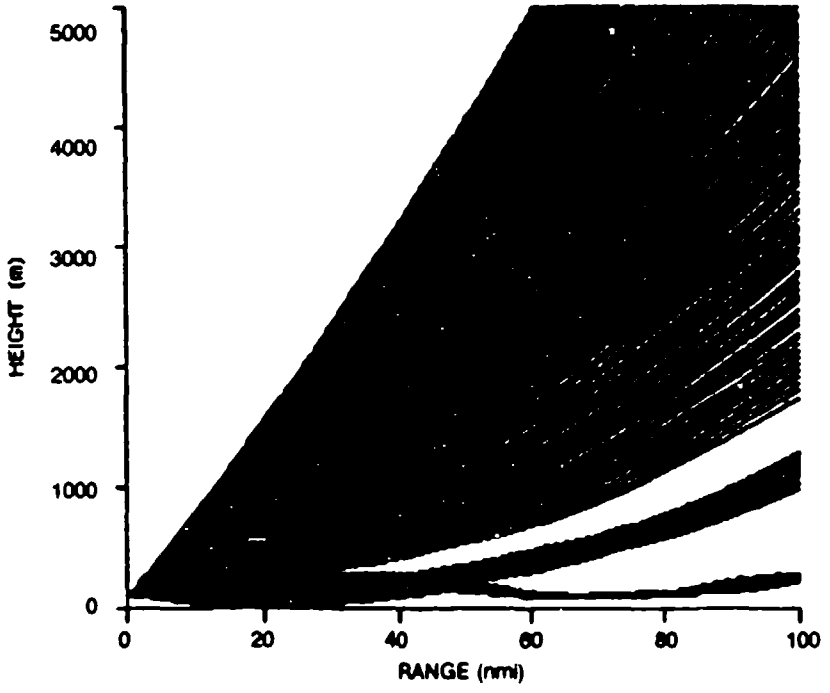

ANT HT m	100
# of RAYS	200
MIN ANG mrad	-4.9
MAX ANG mrad	37.5
REFLECTED RAYS	Y

PROFILE

HEIGHT (m)	M-UNITS
0.0	315.0
150.0	332.4
225.0	345.4
285.0	325.7
307.5	357.2
337.5	327.9
375.0	348.9
412.5	352.7
480.0	348.6
517.5	356.5
600.0	344.6
705.0	376.7
810.0	390.0
900.0	396.0
1005.0	419.4

Figure A3. (Continued.) Data for 20 September 1989.

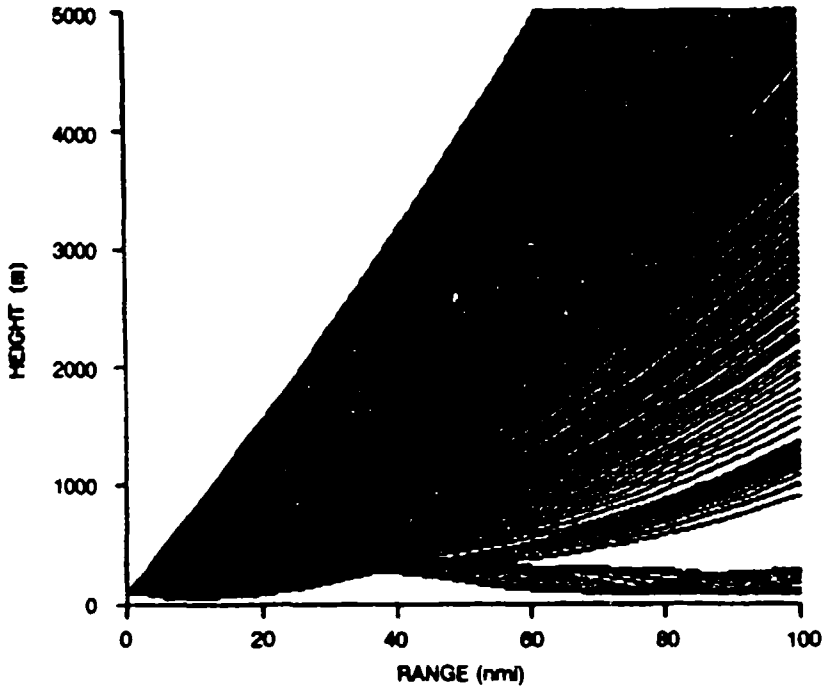

ANT HT m	100
# of RAYS	200
MIN ANG mrad	-4.9
MAX ANG mrad	37.5
REFLECTED RAYS	Y

PROFILE

HEIGHT(m)	M-UNITS
0.0	340.0
123.3	367.5
232.6	382.8
269.4	382.6
285.3	381.7
326.1	380.0
410.4	372.2
500.2	378.1
615.8	388.3
701.3	397.0
806.1	409.4
883.3	419.0
936.1	425.7
982.5	430.1
1011.5	433.8

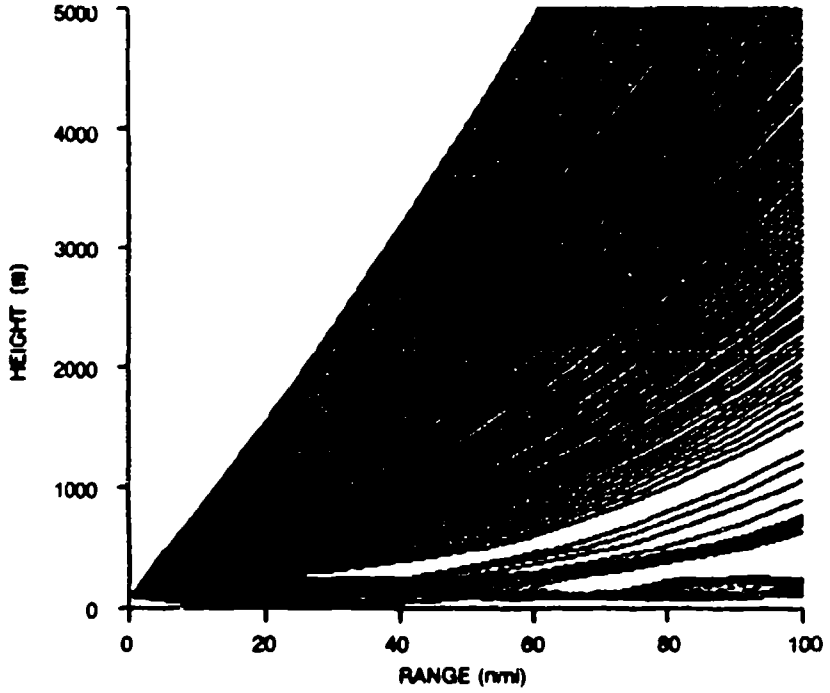

ANT HT m	100
# of RAYS	200
MIN ANG mrad	-4.9
MAX ANG mrad	37.5
REFLECTED RAYS	Y

PROFILE

HEIGHT(m)	M-UNITS
0.0	340.0
105.0	348.7
150.0	357.1
210.0	369.0
262.0	345.9
300.0	351.7
405.0	356.5
510.0	369.5
600.0	379.9
705.0	392.8
810.0	404.3
900.0	407.4
952.5	419.4
975.0	420.2
1005.0	423.9

Figure A3. (Continued.) Data for 27 September 1989.

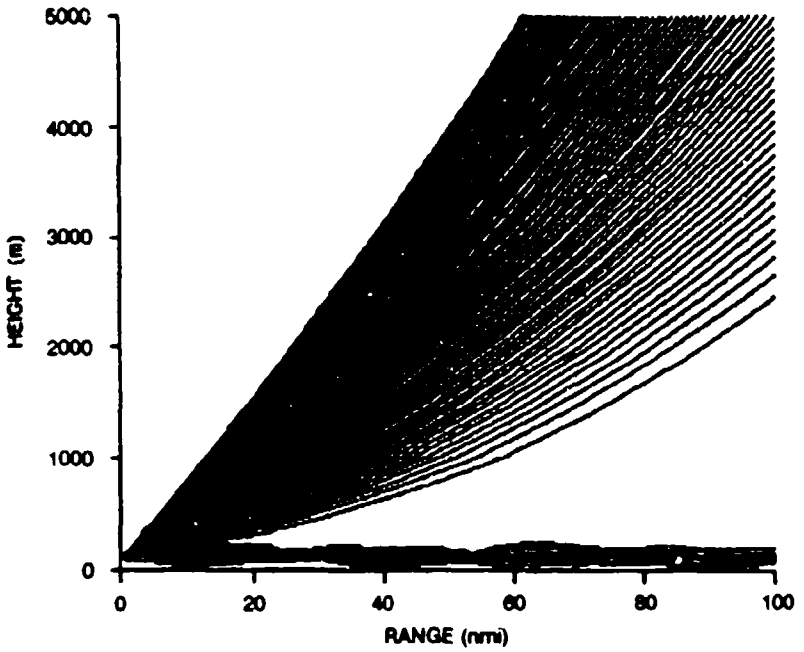

ANT HT m	100
# of RAYS	100
MIN ANG mrad	-4.9
MAX ANG mrad	37.5
REFLECTED RAYS	Y

PROFILE

HEIGHT(m)	M-UNITS
0.0	330.0
45.6	359.1
169.2	371.8
255.0	384.8
350.4	386.6
383.7	389.0
400.0	387.9
452.6	390.6
490.1	392.9
540.6	394.1
660.0	399.9
752.6	407.5
854.5	420.3
926.8	428.2
1002.6	450.2

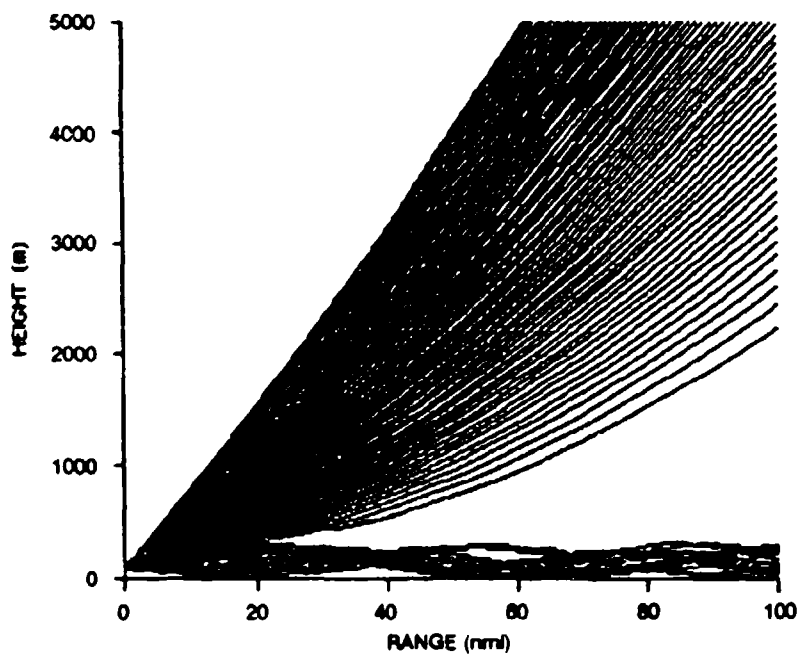

ANT HT m	100
# of RAYS	100
MIN ANG mrad	-4.9
MAX ANG mrad	37.5
REFLECTED RAYS	Y

PROFILE

HEIGHT(m)	M-UNITS
0.0	330.0
97.5	344.2
172.5	361.9
187.5	365.6
262.5	339.5
277.5	345.4
322.5	324.8
397.5	346.3
450.0	326.3
480.0	347.0
525.0	358.9
660.0	376.1
802.0	391.2
900.0	401.0
1005.0	415.5

Figure A3. (Continued.) Data for 29 September 1989.

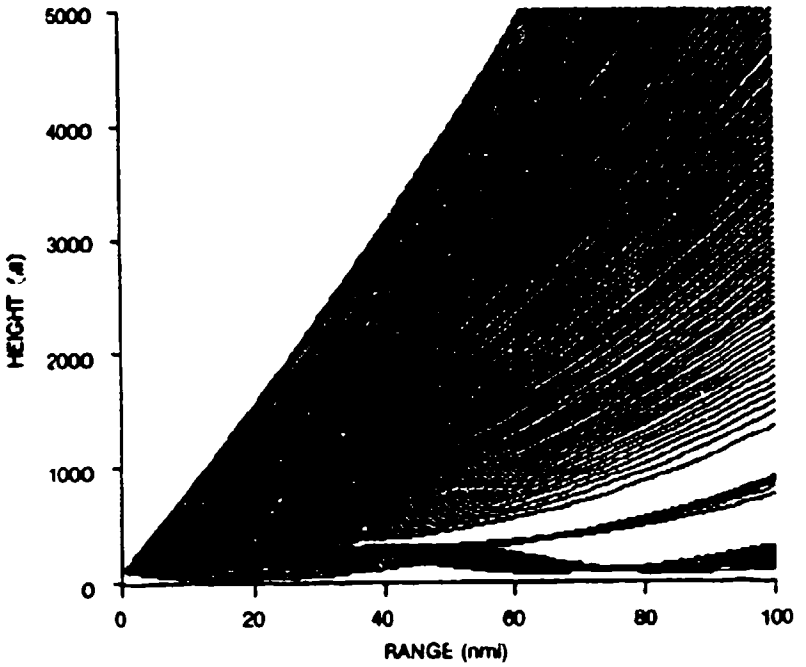

ANT HT m	100
# of RAYS	200
MIN ANG mrad	-4.9
MAX ANG mrad	37.5
REFLECTED RAYS	Y

PROFILE

HEIGHT(m)	M-UNITS
0.0	340.0
180.0	364.0
226.6	370.3
255.9	376.4
285.3	362.9
325.4	349.2
400.0	355.4
450.4	360.1
537.9	371.5
650.0	372.6
801.3	403.0
908.2	410.9
1008.7	414.7

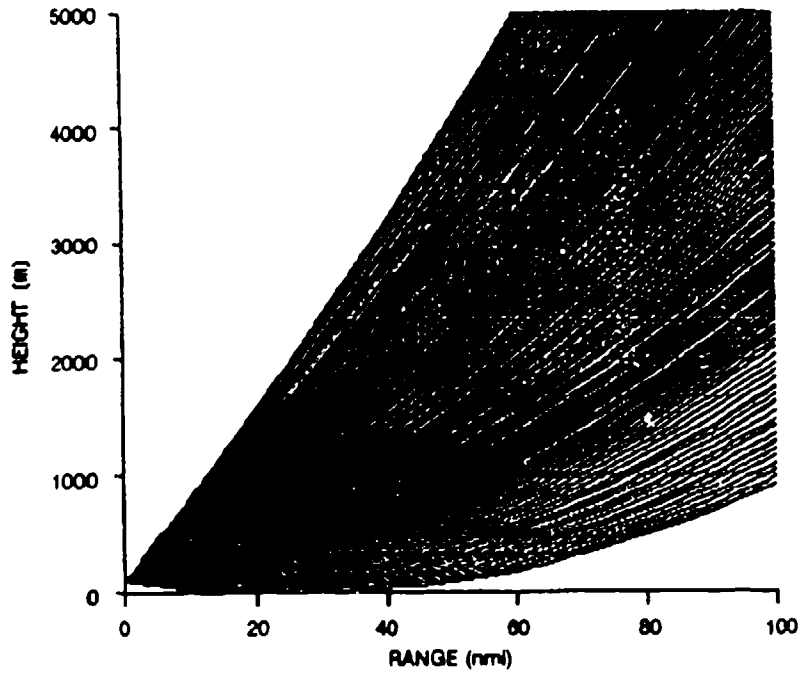

ANT HT m	100
# of RAYS	200
MIN ANG mrad	-4.9
MAX ANG mrad	37.5
REFLECTED RAYS	Y

PROFILE

HEIGHT(m)	M-UNITS
0.0	325.0
105.0	333.7
180.0	348.0
217.5	355.9
270.0	369.3
300.0	353.8
330.0	355.1
405.0	366.8
517.5	374.3
600.0	381.6
705.0	392.5
802.5	407.8
900.0	424.8
960.0	425.5
1005.0	433.3

Figure A3. (Continued.) Data for 21 November 1989.

REPORT DOCUMENTATION PAGE

Form Approved
OMB No. 0704-0188

1 AGENCY USE ONLY (Leave blank)	2 REPORT DATE	3 REPORT TYPE AND DATES COVERED
	January 1990	Final: FY 1989–1990

4 TITLE AND SUBTITLE

RADIO REFRACTIVITY PROFILES DEDUCED FROM LIDAR MEASUREMENTS

5 FUNDING NUMBERS

PE: 62435N
WU: DN488 760

6 AUTHOR(S)

M. R. Paulson, H. G. Hughes

7 PERFORMING ORGANIZATION NAME(S) AND ADDRESS(ES)

Naval Ocean Systems Center
Code 543
San Diego, CA 92152-5000

8 PERFORMING ORGANIZATION REPORT NUMBER

NOSC TD 1752

9 SPONSORING/MONITORING AGENCY NAME(S) AND ADDRESS(ES)

Naval Ocean Systems Center
San Diego, CA 92152-5000

10 SPONSORING/MONITORING AGENCY REPORT NUMBER

11 SUPPLEMENTARY NOTES

12a DISTRIBUTION/AVAILABILITY STATEMENT

Approved for public release; distribution is unlimited.

12b DISTRIBUTION CODE

13 ABSTRACT (Maximum 200 words)

Measurements are presented of the returns from a vertically pointing lidar, along with simultaneous radiosonde measurements of meteorological parameters on 13 cloud-free days near the ocean at San Diego, California. Linear regression analyses between the lidar range-compensated power, S(R), and the relative humidity, RH, gave high coefficients of correlation for individual days, but the magnitudes of the regression constants differed from day to day, indicating differing properties of the aerosols for each day. The combined data set was used to derive a linear relationship between S(R) at different altitudes and the corresponding values of RH. This resulted in a correlation coefficient of 0.73. Using standard vertical lapse rates of temperature and pressure with the profiles of relative humidity determined from the lidar returns, the modified radio refractivity (M-units) variations with altitude were determined for each of the days. These M-unit profiles were then compared to the corresponding values calculated from the radiosonde data. While the absolute values differed with altitude in most cases, the gradients in M-units with altitude corresponded remarkably well. Using a ray-trace computer program, two-dimensional (altitude-versus-range) plots of the radio signal coverage were determined by using the M-unit profiles determined by the two methods. The plots in both cases show similar ducting conditions. The results of this study show that a lidar may be a valuable supplemental tool in estimating radio wave ducting conditions from aboard ship during cloud-free days when controlled electromagnetic emission conditions prohibit the launching of radiosondes. Additional data are required to test the utility of the regression relationship between S(R) and RH in locations other than Southern California.

14 SUBJECT TERMS

propagation, electromagnetic emission, lidars, radio refractivity, meteorology, radiosondes, ducting, ray-trace computer programs, emission control (EMCON)

15 NUMBER OF PAGES

39

16 PRICE CODE

17 SECURITY CLASSIFICATION OF REPORT	18 SECURITY CLASSIFICATION OF THIS PAGE	19 SECURITY CLASSIFICATION OF ABSTRACT	20 LIMITATION OF ABSTRACT
UNCLASSIFIED	UNCLASSIFIED	UNCLASSIFIED	SAME AS REPORT